The Astrophysical Journal, 816:86 (19pp), 2016 January 10 doi:10.3847/0004-637X/816/2/86

MERGERS AND STAR FORMATION: THE ENVIRONMENT AND STELLAR MASS GROWTH OF THE PROGENITORS OF ULTRA-MASSIVE GALAXIES SINCE $Z = 2$

Benedetta Vulcani[1], Danilo Marchesini[2], Gabriella De Lucia[3], Adam Muzzin[4], Mauro Stefanon[5], Gabriel B. Brammer[6], Ivo Labbé[5], Olivier Le Fèvre[7], and Bo Milvang-Jensen[8]
[1] Kavli Institute for the Physics and Mathematics of the Universe (WPI), The University of Tokyo Institutes for Advanced Study (UTIAS), the University of Tokyo, Kashiwa, 277-8582, Japan; benedetta.vulcani@ipmu.jp
[2] Department of Physics and Astronomy, Tufts University, Medford, MA 02155, USA
[3] INAF-Astronomical Observatory of Trieste, I-34143 Trieste, Italy
[4] Institute of Astronomy, University of Cambridge, Madingley Road, Cambridge CB3 0HA, UK
[5] Leiden Observatory, Leiden University, P.O. Box 9513, 2300 RA Leiden, The Netherlands
[6] Space Telescope Science Institute, 3700 San Martin Drive, Baltimore, MD 21218, USA
[7] Aix Marseille Université, CNRS, Laboratoire d'Astrophysique de Marseille, UMR 7326, F-13388, Marseille, France
[8] Dark Cosmology Centre, Niels Bohr Institute, University of Copenhagen, Juliane Maries Vej 30, DK-2100 Copenhagen, Denmark
Received 2015 August 31; accepted 2015 November 18; published 2016 January 14

ABSTRACT

The growth of galaxies is a key problem in understanding the structure and evolution of the universe. Galaxies grow their stellar mass by a combination of star formation and mergers, with a relative importance that is redshift dependent. Theoretical models predict quantitatively different contributions from the two channels; measuring these from the data is a crucial constraint. Exploiting the UltraVISTA catalog and a unique sample of progenitors of local ultra-massive galaxies selected with an abundance matching approach, we quantify the role of the two mechanisms from $z = 2$ to 0. We also compare our results to two independent incarnations of semi-analytic models. At all redshifts, progenitors are found in a variety of environments, ranging from being isolated to having 5–10 companions with mass ratio at least 1:10 within a projected radius of 500 kpc. In models, progenitors have a systematically larger number of companions, entailing a larger mass growth for mergers than in observations, at all redshifts. Generally, in both observations and models, the inferred and the expected mass growth roughly agree, within the uncertainties. Overall, our analysis confirms the model predictions, showing how the growth history of massive galaxies is dominated by in situ star formation at $z \sim 2$, both star formation and mergers at $1 < z < 2$, and by mergers alone at $z < 1$. Nonetheless, detailed comparisons still point out tensions between the expected mass growth and our results, which might be due to either an incorrect progenitors-descendants selection, uncertainties on star-formation rate and mass estimates, or the adopted assumptions on merger rates.

Key words: galaxies: evolution – galaxies: formation – galaxies: general – galaxies: high-redshift

1. INTRODUCTION

Even though in the last decades much attention has been dedicated to the study of galaxy formation and evolution, understanding when and how the most massive galaxies formed and how they evolve with time are still controversial questions. In the standard paradigm of structure formation, dark matter haloes assemble hierarchically in a gravitational collapse, and galaxies form inside these structures following the radiative cooling of baryons. Stars in today's most massive galaxies ($M_* \sim 10^{12}\ M_\odot$) are formed very early (50% at $z \sim 5$, 80% at $z \sim 3$) and in many small galaxies. Model massive galaxies can have a number of effective progenitors as high as ∼5 and assemble surprisingly late. Predictions are model dependent; according to De Lucia et al. (2006) and De Lucia & Blaizot (2007) half their final mass is typically locked-up in a single galaxy after $z \sim 0.5$.

Many physical processes have to be taken into account to explain the growth of massive galaxies. Star formation is expected to play an important role at higher redshifts because a large fraction of massive galaxies at $z \sim 2$ have high star-formation rates (SFRs; e.g., van Dokkum et al. 2004; Papovich et al. 2006). However, the old stellar ages of the most massive early-type galaxies (e.g., Thomas et al. 2005; van Dokkum & van der Marel 2007) and the existence of apparently "red and dead" galaxies with small sizes at $z = 1.5$–2.5 (e.g., Cimatti et al. 2008; van Dokkum 2008) suggest that at least some of the growth is due to other mechanisms, like mergers. Recently, Graham (2013), Dullo & Graham (2013), and Graham et al. (2015) have also suggested that some massive galaxies have evolved by accreting a large disc of gas that rapidly forms stars rather than growth only via mergers.

Below $z \sim 1$, most massive galaxies ($M_* \sim 10^{12}\ M_\odot$) are generally found in dense environments (Blanton & Moustakas 2009), such as at the center of clusters, and are identified as the Brightest Cluster Galaxies (BCGs). Nonetheless, the recent survey MASSIVE (Ma et al. 2014) showed that this might not be always the case. They observed 116 galaxies with $M_* \sim 10^{11.5}\ M_\odot$ and distance $D < 108$ Mpc ($z < 0.025$) finding that 48%–56% of them were located in groups (35%–38% are actually central galaxies), while 6%–14% were isolated. Many studies have focused on characterizing the assembly of massive galaxies, both from a theoretical and observational point of view. Lidman et al. (2012) and Lin et al. (2013) found that the stellar mass of BCGs increases by a factor of ∼2 since $z \sim 1$. SFRs in BCGs at $z \sim 1$ are generally too low to result in significant amounts of mass. Instead, most of the mass build up occurs through mergers. In semi-analytic models, the accretion of satellite galaxies is mainly dry and minor (e.g., De Lucia & Blaizot 2007), whereas in observations many works point to major mergers in the center of clusters as the main reason of the mass growth (Rasmussen et al. 2010; Brough et al. 2011; Bildfell et al. 2012; Lidman et al. 2013).

Characterizing three BCGs at $z \sim 0.1$ with nearby companions, Brough et al. (2011) found that the companions of two of the BCGs would merge with the BCG within 0.35 Gyr. Additional examples of likely major mergers can be found in Rasmussen et al. (2010), Yamada et al. (2002), and Collins et al. (2009). While it is clear that mergers do occur, it is not yet clear what fraction of the stars in the merging galaxies ends up in the BCG and what fraction is distributed throughout the cluster. High-resolution simulations suggest that between 50% and 80% of the mass of mergers is not locked into galaxies, but is distributed throughout the cluster (Conroy et al. 2007; Puchwein et al. 2010). Recent observational studies, on the basis of color gradients, support simulations that claim that at least half of the mass is lost into the intracluster medium of the clusters (e.g., Lidman et al. 2012; Burke et al. 2015).

At higher redshift, the environment in which massive galaxies reside is less characterized, and a clear correspondence between massive galaxies and BCGs is lacking. Nonetheless, a number of studies have characterized the build up of massive galaxies. Ownsworth et al. (2014), using a variety of number density selections, claimed that more than half of the total stellar mass in massive galaxies ($M_* \sim 10^{11.24} M_\odot$) at $z = 0.3$ is created externally to the $z = 3$ progenitors. van Dokkum et al. (2010), selecting galaxies at a constant number density of $n = 2 \times 10^{-4}\,\mathrm{Mpc}^{-3}$, found that the role of mergers might be even more important, with star formation accounting only for 20% of the total mass growth. Connecting high and low-redshift BCG data via evolution of their host halo masses, Shankar et al. (2015) found an increase since $z \sim 1$ of a factor ~2–3 in their mean stellar mass and ~2.5–4 in their mean effective radius.

To really understand how individual galaxies have evolved and assembled their mass and what mechanisms drive these changes, it is important to properly connect today's most massive galaxies to their progenitors at earlier times. This requires the non-trivial task of linking galaxies and their descendants/progenitors through cosmic time, which in turn requires assumptions for how galaxies evolve. In recent years, a few approaches have been developed to link galaxies across cosmic time (e.g., Wake et al. 2006; Conroy & Wechsler 2009; Brammer et al. 2011; Behroozi et al. 2013; Leja et al. 2013; Mundy et al. 2015). Whereas the limitations of these techniques are still being debated (e.g., Torrey et al. 2015), it is widely recognized that these approaches are far superior than selecting galaxies at fixed stellar mass for studies of galaxy evolution.

Marchesini et al. (2014) assembled the first sample of galaxies defined to be the progenitors of galaxies with $\log M_*/M_\odot > 11.8$ at $z = 0$ (ultra-massive galaxies, hereafter UMGs) from $z = 3$ using a semi-empirical approach based on abundance matching in the ΛCDM paradigm (Behroozi et al. 2013, see Section 2.1). Characterizing the stellar population properties of the progenitors (masses, ages, dust star formation), they claimed that at least half of the stellar content of local UMGs was assembled at $z > 1$, whereas the remaining was assembled via merging from $z \sim 1$ to the present. They also found that most of the quenching of the star-forming progenitors happened between $z = 2.75$ and $z = 1.25$, which is in good agreement with the typical formation redshift and scatter in age of $z = 0$ UMGs as derived from their fossil records. The progenitors of local UMGs, including the star-forming ones, never lived on the blue cloud since $z = 3$.

Using the unique progenitor-descendant sample presented in Marchesini et al. (2014), in this paper we focus on the environment in which these progenitors reside and test whether their mass growth can be ascribable mainly to mergers or to star formation. In particular, we explicitly test the model predictions for the different contributions to the stellar mass assembly since $z \sim 2$. Both semi-analytic models (e.g., Zehavi et al. 2012) and abundance matching techniques based on halo occupation models (e.g., Conroy & Wechsler 2009) indicate that star formation is important at all halo masses at $z \sim 2$; at $z < 1$ accretion through mergers dominates at the high-mass end ($\sim 10^{13}\,\mathrm{h}^{-1}\,M_\odot$) of the halo mass distribution, where star formation is negligible, while at intermediate redshift both contributions are important. Solving possible discrepancies found between observations and simulations is beyond the scope of this paper, and is deferred to a forthcoming analysis.

We parameterize the environment in terms of projected distance from the progenitor because we have no information about the mass of the haloes in which these galaxies reside. We only consider mergers between galaxies with a mass ratio at most of 1:10. We also compare our observational results to the predictions of two semi-analytic models, namely the De Lucia & Blaizot (2007, hereafter DLB07) and the Henriques et al. (2015, hereafter H15) model, to investigate whether the Marchesini et al. (2014) approach to link galaxies across cosmic time is supported by these models.

Throughout the paper, we assume $H_0 = 70\,\mathrm{km\,s^{-1}\,Mpc^{-1}}$, $\Omega_0 = 0.3$, and $\Omega_\Lambda = 0.7$. We adopt a Kroupa (2001) initial mass function (IMF) in the mass range 0.1–100 $M_\odot$.

2. DATA SET

Our sample is drawn from the K_S-selected catalog of the COSMOS/UltraVISTA field from Muzzin et al. (2013a). The catalog covers $1.62\,\mathrm{deg}^2$ and includes point-spread function-matched photometry in 30 photometric bands over the wavelength range 0.15–24 μm from the available *GALEX* (Martin et al. 2005), Canada–France–Hawaii Telescope/Subaru (Capak et al. 2007), UltraVISTA (McCracken et al. 2012), and S-COSMOS (Sanders et al. 2007) data sets. Sources are selected from the DR1 UltraVISTA K_S-band imaging (McCracken et al. 2012), which reaches a depth of $K_{S,\,\mathrm{tot}} < 23.4$ at 90% completeness. Details on the photometric catalog construction, photometric redshift measurements, and stellar population properties' estimates can be found in Muzzin et al. (2013a). Briefly, stellar population properties were derived by fitting the observed spectral energy distributions (SEDs) from the *GALEX* UV to the *Spitzer*-IRAC 8 μm photometry with Bruzual & Charlot (2003) models assuming exponentially declining SFHs of the form $\mathrm{SFR} \propto e^{-t/\tau}$, where t is the time since the onset of star formation and τ sets the timescale of the decline in the SFR, solar metallicity, a Calzetti et al. (2000) dust law, and a Kroupa (2001) IMF (see also Marchesini et al. 2014).

Marchesini et al. (2014) investigated the effects of different SED-modeling assumptions by adopting, among others, different SFHs and metallicities. Adopting a delayed-τ SFH in place of the exponentially declining SFH allows for increasing SFR at earlier times. The delayed-τ model implies SFRs that are smaller by ~0.1 dex and stellar ages $\langle t \rangle_{\mathrm{SFR}}$ that are larger by $\tau \sim 0.1$ dex compared with the default SED-modeling assumptions. Relaxing the assumption on metallicity

by leaving it as a free parameter in the SED modeling does not noticeably change the result, indicating that the impact of fixing the metallicity to the solar one is almost negligible. Overall, the systematic effects on the stellar population properties are found to be significantly smaller than the corresponding typical random uncertainties for most of the different SED-modeling assumptions. Therefore, results are robust and not very sensitive to reasonable choices of the SED-modeling assumptions.

The redshift-dependent stellar mass-completeness limit has been presented in Muzzin et al. (2013b). This was determined by selecting galaxies belonging to the available deeper samples and then scaled fluxes and $M_\star$ to match the K-band completeness limit of the UltraVISTA sample ($K_{S,\ \mathrm{tot}} = 23.4$). The upper envelope of points in the ($M_{\star,\mathrm{scaled}}$–$z$) space represents the most massive galaxies at $K_S = 23.4$, and so provides a redshift-dependent 100% $M_\star$ completeness limit for the UltraVISTA sample. Similarly, Muzzin et al. (2013b) also derived 95% mass-completeness limits for the sample, which increases the sample by a factor of 1.4. Given this substantial increase in statistics, we follow Muzzin et al. (2013b) and adopt the 95% mass-completeness limits.

The quiescent/star-forming separation was done using the rest-frame $U - V$ versus $V - J$ color–color diagram and is presented in Muzzin et al. (2013b) and Marchesini et al. (2014). This method has the ability to separate red galaxies that are quiescent from reddened (i.e., dust-obscured) star-forming galaxies (see, e.g., Labbé et al. 2006; Wuyts et al. 2007; Williams et al. 2009; Brammer et al. 2011; Patel et al. 2011; Whitaker et al. 2011; Muzzin et al. 2013a).

2.1. The Selection of the Progenitors of Local UMGs

The progenitors of local UMGs were selected by adopting a semi-empirical approach that uses abundance matching in the ΛCDM paradigm (see Marchesini et al. 2014). This method accounts for mergers and scatter in mass accretion histories. Details on this technique can be found in Behroozi et al. (2013, and references therein). Briefly, the galaxy cumulative number density at redshift z_1 is converted to a halo mass with equal cumulative number density using peak halo mass functions. Then, for haloes at that mass at z_1, the masses of the most massive progenitor haloes at $z_2 > z_1$ are recorded using to the haloes' mass accretion histories. Finally, the median halo progenitor mass at z_2 is converted back into cumulative number densities using the halo mass function at z_2.

The progenitors of the low-z population of very massive galaxies are traced by identifying, at each redshift, the stellar mass for which the evolving cumulative number density intersects the cumulative number density curves derived from the UltraVISTA stellar mass functions (Muzzin et al. 2013a). In this way, a sample of progenitors of galaxies with a mass of $\sim 10^{11.8}\ M_\odot$ at $z \sim 0$ is assembled.

The typical error on the progenitors' stellar mass resulting from the uncertainties of the observed stellar mass functions and cumulative number densities was found to be in the range 0.03–0.07 dex (Marchesini et al. 2014). The inferred growth in stellar mass of the progenitors was therefore found to be 0.45 ± 0.13 dex and 0.27 ± 0.08 dex from $z = 2$ and $z = 1$, respectively, to $z = 0$. If the scatter in mass accretion histories is also included in the error analysis, the uncertainties on the inferred growth in the stellar mass of the progenitors increase by a factor of ∼1.7 (Marchesini et al. 2014).

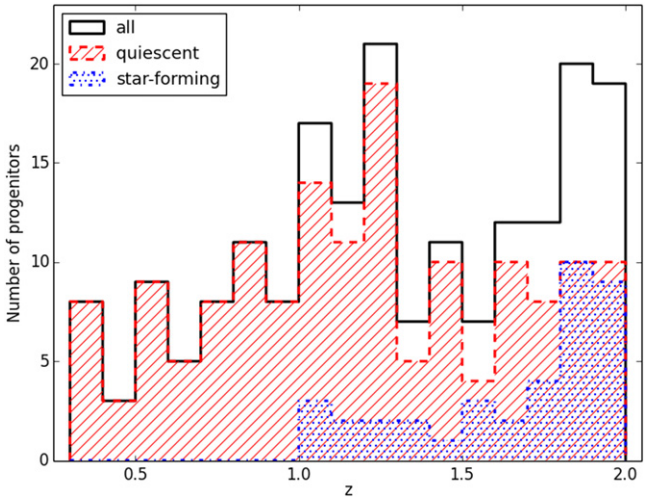

Figure 1. Redshift histogram of our progenitors of UMGs sample (black). The distribution of quiescent (red) and star-forming (blue) galaxies is also shown.

2.2. Our Sample

In this work, we use the sample of progenitors of UMGs defined in Marchesini et al. (2014), but limit our analysis to galaxies at $z < 2$. In this way, at all redshifts, the UltraVISTA sample includes all galaxies at least as massive as 1:10 the mass of the closest progenitor in the redshift range $\pm 0.05 \times (1 + z_{\mathrm{pr}})$ with z_{pr} the photo-z of the progenitor. The redshift range is chosen to take into account the typical photo-z accuracy, which is redshift dependent (see, e.g., Muzzin et al. 2013b). Our selection included 191 progenitors. As shown in Figure 1, the number of progenitors depends on redshift: there are 11 galaxies at $0.2 < z < 0.5$; 41 at $0.5 < z < 1$; 69 at $1 < z < 1.5$; and 70 at $1.5 < z < 2$. The different frequency is mainly due to the different volume covered by the different redshift bins, which is ∼10× larger at $z \sim 1.75$ than at $z \sim 0.35$. Indeed, the volume probed is $\sim 25\ \mathrm{Gpc}^3$ at $0.2 < z < 0.5$; $\sim 125\ \mathrm{Gpc}^3$ at $0.5 < z < 1$; $\sim 200\ \mathrm{Gpc}^3$ at $1 < z < 1.5$; and $\sim 235\ \mathrm{Gpc}^3$ at $1.5 < z < 2$.

As already noted by Marchesini et al. (2014), at $z < 1$ all galaxies are quiescent, whereas at higher redshift the fraction of star-forming progenitors is not negligible.

To characterize the environment in which progenitors are embedded, we also make use of the entire UltraVISTA catalog, to which we apply a mass cut to ensure 95% completeness (see Section 2).

Hereafter, we refer to those galaxies around the progenitors within a specified projected radius, at least as massive as 1:10 the mass of the progenitor, and in the redshift range $\pm 0.05 \times (1 + z_{\mathrm{pr}})$ as *companion* galaxies.

We note that there might be systematic effects in the data that alter the robustness of the results, such as systematic errors in photometric redshifts and contamination of the photometry from emission lines. The latter might result in overestimates of stellar masses. Marchesini et al. (2014) investigated the possible systematics in the UltraVISTA sample and showed that they should not impact our findings at the redshifts considered here (see also Muzzin et al. 2013a).

3. THEORETICAL PREDICTIONS

In this paper, to investigate the physical processes implemented in the models, we compare findings from the observations with the predictions from theoretical models on the environment of the progenitors of today's UMGs, as well as on the relative importance of merging versus in situ star formation to their inferred growth in stellar mass. To this aim, the model predictions are derived in two different ways. In one case, the model-predicted assembly histories of the progenitors are directly exploited to determine the overall growth in stellar mass of the descendants. In the other case, the growth in stellar mass is obtained following the same assumptions used in the observations.

We exploit galaxy catalogs from two semi-analytic models run on the Millennium Simulation (Springel et al. 2005). This uses 10^{10} particles of mass $8.6 \times 10^8\,h^{-1}\,M_\odot$ to trace the evolution of the matter distribution in a cubic region of the universe of $500\,h^{-1}$ Mpc on a side from $z = 127$ until $z = 0$, and has a spatial resolution of $5\,h^{-1}$ kpc.

We use two different semi-analytic models to investigate how different assumptions about the physical processes acting on the baryonic component impact the evolution of the galaxy masses.

The semi-analytic model discussed in DLB07 builds on the methodology and prescriptions introduced in Springel et al. (2001), De Lucia et al. (2004b), and Croton et al. (2006) and was the first variant of the "Munich" model family to be made publicly available. The DLB07 model is based on WMAP1 cosmology (Sánchez et al. 2006) and includes prescriptions for supernova-driven winds, follows the growth of supermassive black holes, and includes a phenomenological description of active galactic nucleus (AGN) feedback. The model neglects environmental physical processes such as ram pressure and harassment, but assumes that when galaxies are accreted onto a more massive system, the associated hot gas reservoir is stripped instantaneously. This induces a very rapid decline of the star-formation histories of satellite galaxies, and contributes to creating an excess of red and passive galaxies with respect to the observations (e.g., Wang et al. 2007). The DLB07 model is mainly tuned to reproduce the K-band luminosity function at $z = 0$.

We also use the model presented in H15, which represents one of the most recent updates of the Munich models. The H15 model uses the Planck first-year cosmology and basically contains the same physics as the DLB07 model but has a more sophisticated treatment for the evolution of satellites. In a change from the DLB07 model, which does not include a channel for ICL formation, the H15 model includes tidal stripping as a channel for ICL. In addition, it adds a modification of the timescale to re-accrete gas ejected through galactic winds and modifies the ram-pressure stripping in haloes less massive than $\sim 10^{14}\,M_\odot$. The model is tuned to reproduce recent data on the abundance and passive fractions of galaxies and the galaxy stellar mass function from $z = 3$ down to $z = 0$. We refer to the original papers for more details.

As explained in Springel et al. (2001) and De Lucia et al. (2004a), models make a distinction between centrals, satellites, and orphans. Centrals (type 0) are located at the position of the most bound particle in their halo. These galaxies are fed by gas cooling from the surrounding hot halo medium. Satellites (type 1) were previously central galaxies of another halo, which then merged to form the larger system in which they currently reside. For these galaxies, gas is no longer able to cool onto halo galaxies. Orphans (type 2) are galaxies that are no longer associated with distinct dark matter substructures, and in the DLB07 model their stellar mass is not affected by the tidal stripping that reduces the mass of their parent haloes. In the H15 model, such orphans are unable to retain the gas ejected by supernova feedback, which is moved to the hot halo of the galaxy group. Tidal forces can completely disrupt the stellar and cold gas components of orphan galaxies, which are then added to the intracluster light and the hot gas atmosphere of the group/cluster, respectively. In both models, orphans may later merge into the central galaxy of their halo. In our analysis, when useful, we will distinguish among the three types of galaxies.

3.1. Our Sample

For both the DLB07 and the H15 models, we extract from the available catalogs all the galaxies at $z = 0.36$, 0.76, 1.28, and 1.77 with stellar mass in the same mass range spanned by the progenitors at the corresponding redshift (approximately within ± 0.15 the median mass of the progenitors).

Since observed masses might be characterized by systematic errors; we also extracted samples of galaxies from the DLB07 model to test the impact of these errors. We assigned to each galaxy mass in the models a random Gaussian error with width $0.03 \times (1 + z)$ (following Ilbert et al. 2013) and then considered only those galaxies whose perturbed mass was in the mass range ± 0.15 the stellar mass of the progenitors at the corresponding redshift. We performed the entire analysis using both samples, without finding noticeable differences between the results. Therefore, in the following, we present only the analysis performed on the sample with the original masses from the models.

Overall, in the DLB07 (H15) model 1027 (1076) galaxies have been extracted at $z = 0.36$, 608 (1231), at $z = 0.76$, 447 (1969), and at $z = 1.28$ and 311 (1732) at $z = 1.77$.

From the models, we also extract the information regarding the merger trees and the descendants of these galaxies down to $z \sim 0$, with the aim of investigating the real mass growth predicted by the models. In addition, we also get the virial mass of the haloes in which these galaxies reside and those of their descendants, to further characterize the progenitors' hosting environment, from a theoretical point of view.

Finally, we select all galaxies within a box of one physical Mpc on a side, centered on each massive galaxy considered, in order to characterize the environment of the progenitors of UMGs in the same way as in observations.

4. DESCENDANTS OF THE PROGENITORS IN THE MODELS

We test whether the models support the approach adopted by Marchesini et al. (2014) to link galaxies across the cosmic time.

From simulations, we randomly extract the same number of progenitors found in observations at the corresponding redshift and compute the median mass of their descendants at $z \sim 0$. We repeat the sampling 10 times to take into account sample variance. Figure 2 shows that the selection based on the abundance matching method does indeed select galaxies whose mass evolution is consistent with what is expected from the DLB07 model: Progenitors at the different redshifts will turn

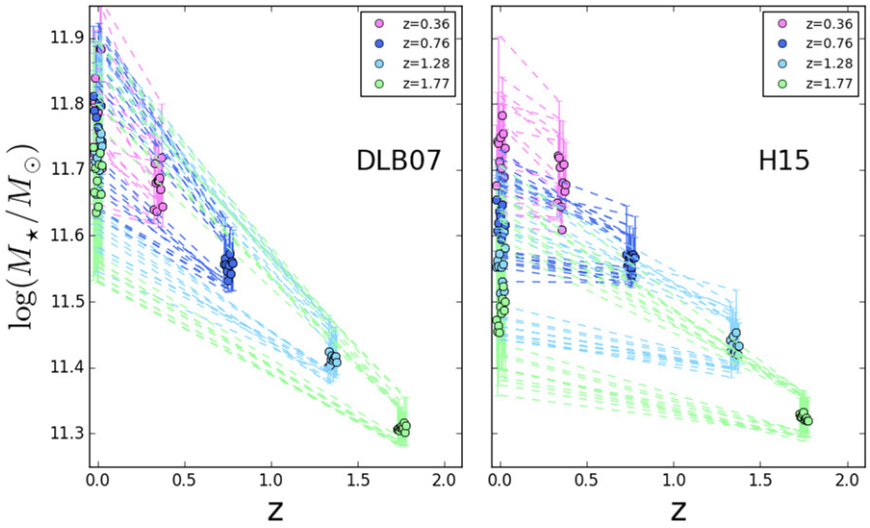

Figure 2. Predicted median progenitor mass growth by semi-analytic models (left: DLB07, right: H15) for galaxies in the same mass range of our progenitors. Masses at $z = 0$ are the masses of the descendants. Error bars on the y-axis represent the 25th and 75th percentiles. At each redshift, 10 random extractions have been performed.

Table 1
Percentages of Type 0, Type 1, and Type 2 Galaxies Among the Progenitors and Descendants in the Two Semi-analytic Models

z	DLB07						H15					
	% Progenitors			% Descendants			% Progenitors			% Descendants		
	type 0	type 1	type 2	type 0	type 1	type 2	type 0	type 1	type 2	type 0	type 1	type 2
0.36	91^{+1}_{-1}	8^{+1}_{-1}	$1.2^{-0.4}_{+20.6}$	88^{+1}_{-1}	6^{+1}_{-1}	6^{+1}_{-1}	85^{+1}_{-1}	12^{+2}_{-1}	$2.9^{+0.8}_{-0.7}$	85^{+2}_{-2}	11^{+1}_{-1}	$4.1^{+1.0}_{-0.8}$
0.76	94^{+1}_{-1}	6^{+1}_{-1}	$0.5^{+0.7}_{-0.3}$	87^{+2}_{-2}	6^{+1}_{-1}	7^{+1}_{-1}	87^{+1}_{-1}	10^{+1}_{-1}	$2.9^{+0.8}_{-0.7}$	86^{+1}_{-1}	10^{+1}_{-1}	$4.3^{+0.9}_{-0.8}$
1.28	93^{+2}_{-2}	6^{+2}_{-1}	$0.9^{+1.0}_{-0.5}$	85^{+2}_{-3}	7^{+2}_{-2}	8^{+2}_{-2}	88^{+1}_{-1}	$8.1^{+0.9}_{-0.8}$	$4.2^{+0.7}_{-0.6}$	84^{+1}_{-1}	12^{+1}_{-1}	$4.5^{+0.7}_{-0.6}$
1.77	95^{+2}_{-2}	4^{+2}_{-1}	$0.6^{+1.0}_{-0.5}$	85^{+3}_{-3}	9^{+3}_{-2}	6^{+2}_{-2}	90^{+1}_{-1}	$6.5^{+0.9}_{-0.8}$	$3.1^{+0.6}_{-0.6}$	85^{+1}_{-1}	11^{+1}_{-1}	$4.6^{+0.8}_{-0.7}$

into galaxies at $z \sim 0$ with masses of $\sim 10^{11.8}\ M_\odot$, which is the mass inferred by Marchesini et al. (2014). The model also reproduces the inferred stellar mass at the intermediate redshifts. By contrast, in the H15 model, the median mass of the descendants at $z = 0$ is lower than $\sim 10^{11.8}\ M_\odot$ in most of the extractions, even within a large dispersion. It is interesting to note that the abundance matching method does not seem to work for the H15 model, even though it is the model that should be in better agreement with the statistics of the halo occupation model by construction (see H15 for details).

Differences between the two models might be due to the fact that H15 introduced tidal stripping and therefore has a smaller number of satellites, producing a smaller mass growth through mergers.

In the following sections we quantify the separate role of star formation and mergers in the galaxy mass growth, also from a purely theoretical point of view, by explicitly inspecting the merger trees of a subsample of galaxies.

Table 1 shows the percentage of galaxies of a given type, for all objects extracted from the simulations. In the DLB07 model, at all redshifts, the vast majority (>90%) of the progenitors are type 0, with the fraction slightly decreasing from higher to lower redshifts. This finding is probably due to the fact that at lower redshift the number of satellites is larger and these galaxies have more time to grow. It suggests that while at higher redshift massive galaxies are most likely at the center of their halo, in the local universe there is a larger fraction of massive galaxies that are satellites. Only $\leqslant$1% are type 2. Among the descendants, the fraction of type 0 is smaller and decreases with increasing redshift of the progenitors, ranging from 85% to 88%. In contrast, the fraction of type 2 galaxies is much larger, and they are as common as satellites (~7% at all redshifts). This suggests that the while almost all massive galaxies that are central at $z = 0.36$ will also be central at $z = 0$, the probability that central galaxies will turn into satellites increases with increasing redshift.

The H15 model presents a systematically lower fraction of type 0 galaxies (85%–90%) and a slightly larger fraction of type 1 among the progenitors, as well as a similar fraction of type 0 and higher fraction of type 1 among the descendants.

Figure 3 shows the halo mass distribution of all the selected progenitors and the mass distribution of the haloes where the descendants of the progenitors reside, for both models. In the DLB07 and H15 prescriptions, the typical mass of the haloes hosting the progenitors increases with decreasing redshift: galaxies at $z = 1.77$ are found in haloes of mass $\sim 10^{12.2}$–$10^{14.6}\ M_\odot$ for the DLB07 model, and of $\sim 10^{12.7}$–$10^{14.7}\ M_\odot$ for the H15 model; galaxies at $z = 0.36$ are found in haloes of mass $\sim 10^{13.4}$–$10^{15.5}\ M_\odot$ for the DLB07 model and of $\sim 10^{13}$–$10^{15.2}\ M_\odot$ for the H15 model. This supports the finding that the growth of the massive galaxies is coupled to the growth of their haloes (e.g., Tinker et al. 2012, and references therein). In the DLB07 model, the halo mass distributions for the descendants span a similar halo mass range, even though the peaks of the distributions slightly depend on the redshift of the progenitors: descendants of the $z = 1.77$ progenitors are found in slightly less massive haloes than the descendants of the $z = 0.36$ progenitors (medians values are

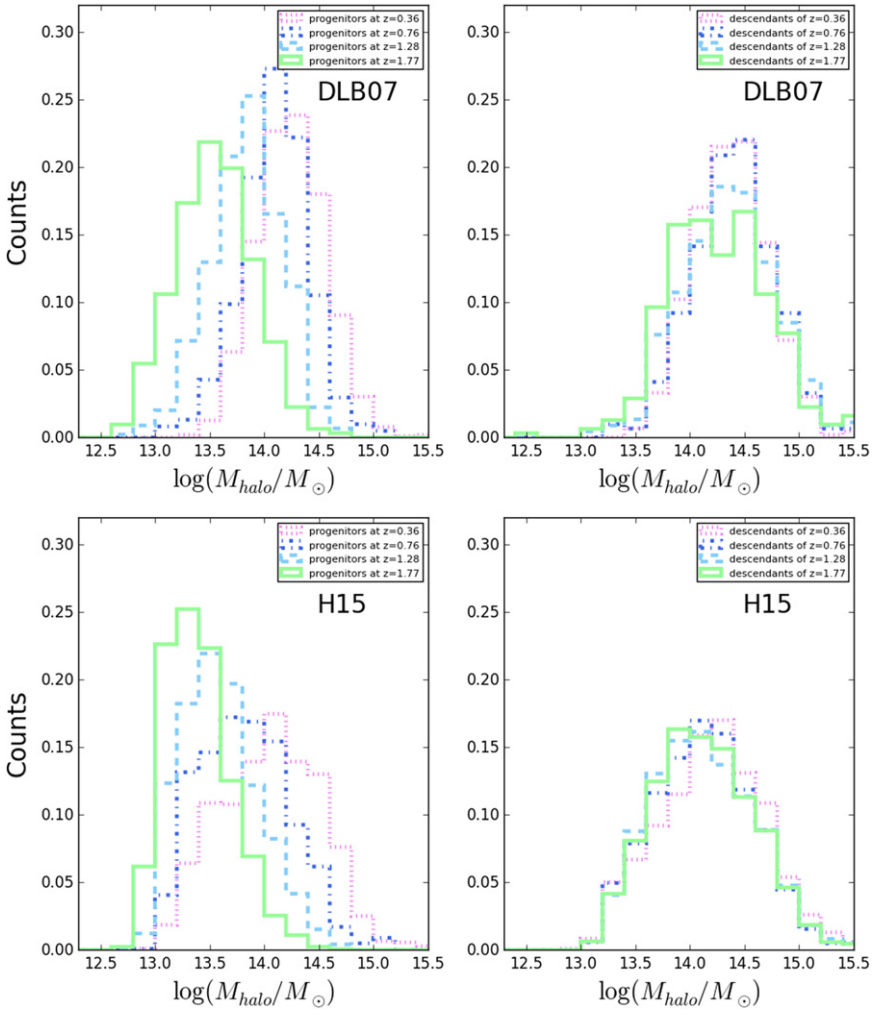

Figure 3. Normalized halo mass distribution for progenitors at different redshfits (left panels) and for their descendants at $z = 0$ (right panels), as indicated in the labels. Upper panels: DLB07 model, bottom panels: H15 model.

$M_{\rm vir} = 10^{14.24\pm0.02}\ M_\odot$, and $M_{\rm vir} = 10^{14.37\pm0.01}\ M_\odot$, respectively). Therefore, even though the progenitors turn into massive galaxies of similar mass, they might not actually end up in the very same galaxies, as shown by the fact that the growth of structure is stochastic. It might also suggest that the environment around the galaxies should be taken into account when linking galaxies across time, and not only the stellar mass. In contrast, in the H15 model, all the descendants span a similar halo mass range ($M_{\rm vir} \sim 10^{13}$–$10^{15.5}\ M_\odot$) with a median halo mass of $10^{14.1\pm0.01}\ M_\odot$. Even though not all the progenitors in the H15 model will end up in massive galaxies as selected by the abundance matching technique, these distributions show that they will end up in very similar environments.

5. THE ENVIRONMENT AROUND THE PROGENITORS OF UMGS

In order to understand the processes that induce the observed galaxy mass growth, we first characterize the environment in which the progenitors of UMGs reside. If these galaxies are found in overdense regions, they should easily undergo mergers; on the other hand, if they are isolated, their growth should be attributable to other factors, such as in situ star formation.

Figure 4 shows some examples of false color images in the BzK filters covering an FOV of 500 kpc on a side of galaxies residing in different environments at different redshifts. In order to demonstrate the range of environments of these galaxies, for each redshift bin, we selected a galaxy with no other companions within a projected sphere of 250 kpc, a galaxy with 3–4 companions, and a galaxy with ∼8–10 companions. Clearly, progenitors reside in a variety of environments, which will have a different role in their growth throughout the cosmic time.

5.1. The Total Number of Satellites Around Progenitors

Using the observed sample drawn from the UltraVISTA catalog, we compute the number of companions around each progenitor at different redshifts. We consider portions of sky that are centered on the progenitor and of different physical radii, and count the number of companions—namely galaxies with mass ratio >1:10 and redshift within the range $\pm0.05 \times (1 + z_{\rm pr})$—that fall into the projected area.

Figure 5 shows the results considering galaxies within 50, 100, 250, and 500 kpc from the progenitor, respectively. According to Muñoz-Cuartas et al. (2011), haloes with $M_{\rm vir} \sim 10^{13}\ M_\odot$ typically have a virial radius of ∼0.5 Mpc below $z \sim 1$, and of ∼0.35 Mpc at $z = 2$, whereas haloes with

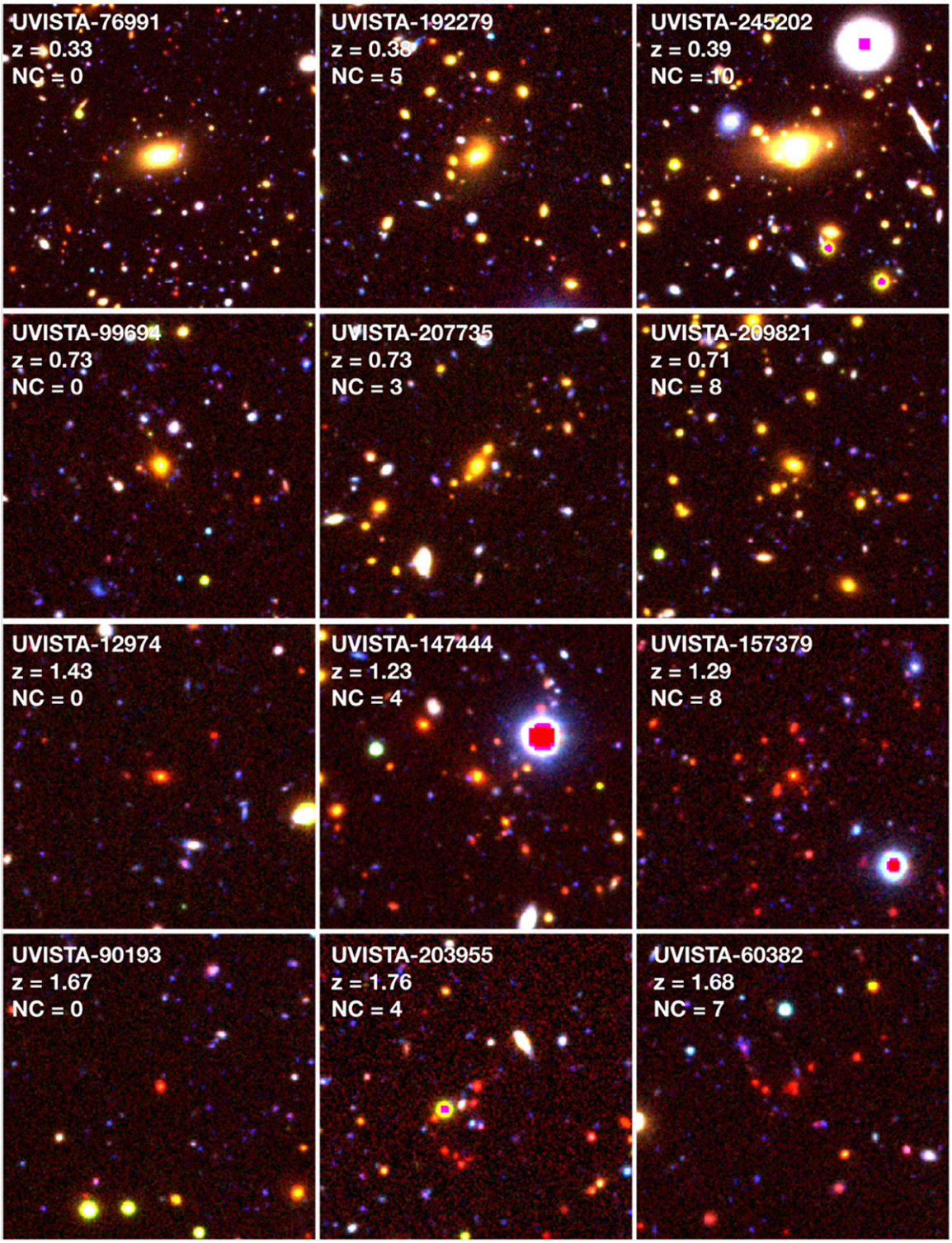

Figure 4. Examples of BzK images for isolated galaxies within 250 kpc (first column), galaxies with few companions (second column), and galaxies with a large number of companions, in four bins of redshifts. Companions are galaxies around the progenitors, at least as massive as ∼1:10 the mass of the progenitor and in the redshift range $\pm 0.05 \times (1 + z_{\rm pr})$. The UltraVISTA id, the redshift, and the number of companions is indicated in the labels. The FOV of each thumbnail corresponds to a radius of 250 kpc.

$M_{\rm vir} \sim 10^{11}\ M_{\odot}$ typically have a virial radius <0.15 Mpc at all redshifts. This binning was chosen to inspect regions of sky that correspond to the virialized region around the progenitors at different redshifts, assuming they are located in a variety of haloes. The smallest distance should sample the virial radius for any progenitor galaxy, while the largest should sample well beyond it.

To get rid of the different volumes covered at the different redshifts and therefore the different number of progenitors, values for each sample are normalized to the total number of progenitors at the considered redshift. In observations (thick lines in both panels), at any redshift, ∼80% of progenitors have no galaxies closer than 50 kpc. At $z < 0.5$ there might be an excess of progenitors with three galaxies within 50 kpc

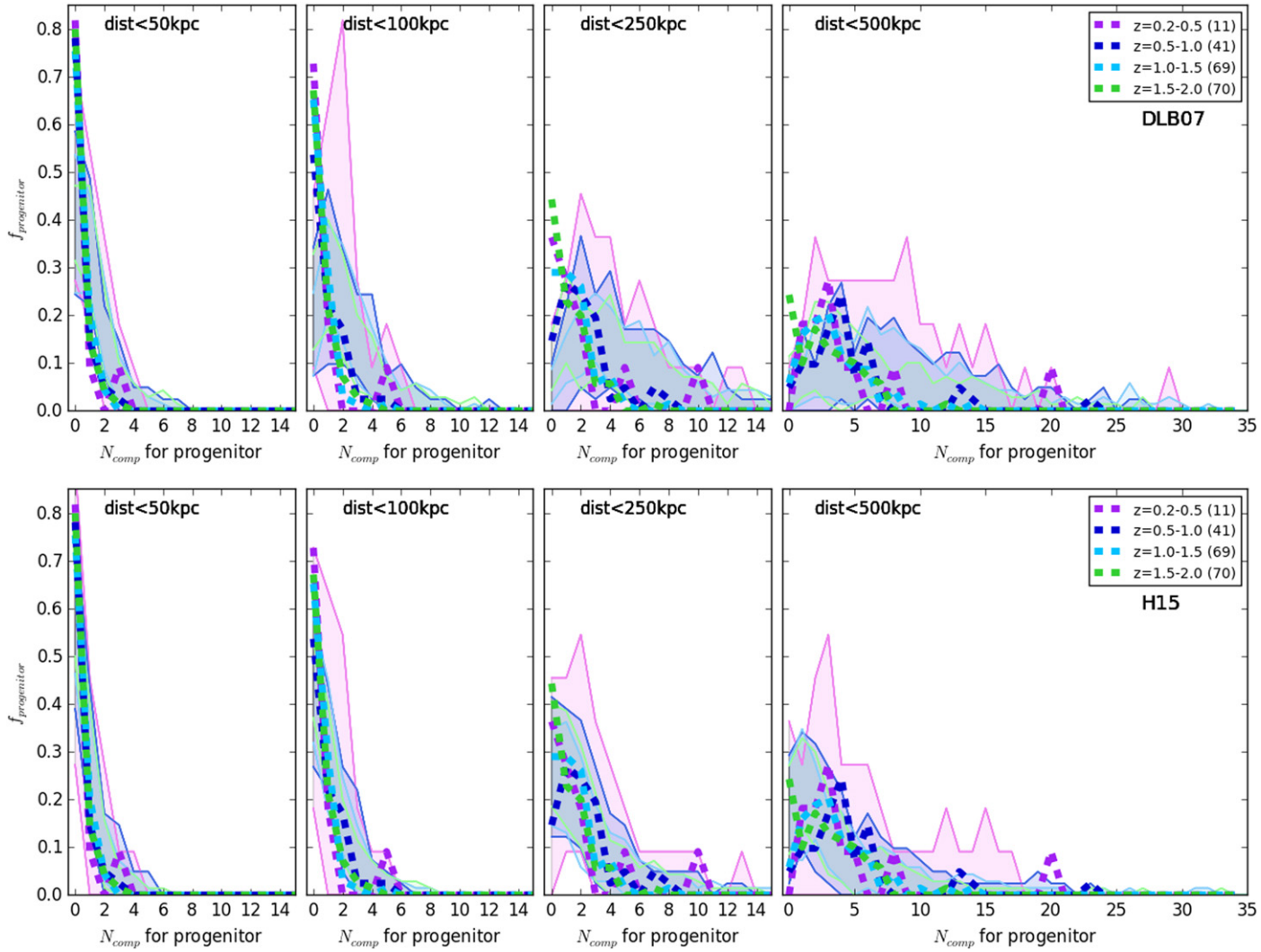

Figure 5. Normalized distribution of the number of companions (i.e., galaxies at least as massive as 1:10 the mass of the progenitor and with z within $\pm 0.05 \times (1 + z_{pr})$) at different redshifts and within different radii (as indicated on the top of each panel). Thick dashed lines represent observations; thin solid lines and shaded areas represent models (upper panels: DLB07, bottom panels: H15). Numbers in parenthesis give the number of progenitors in each redshift bin.

(∼10%). All these progenitors have been found to live in X-ray selected COSMOS groups with halo masses in the range 10^{13}–$10^{14}\,M_{200c}/M_{\odot}$ (George et al. 2011). Enlarging the radius of interest, the number of companions around the progenitors increases and a dependence on redshift might appear for the most extreme galaxies with the largest number of companions. Going from higher to lower redshift, distributions shift toward a larger number of companions, suggesting that the environment around progenitors gets richer. Considering our largest radius (500 kpc), we find that about 25% of progenitors at $1.5 < z < 2$ have no companions and another 25% have at most two companions. On the other hand, at lower redshift 5% of progenitors at most are isolated. At $z < 0.9$, ∼45% of progenitors with at least one companion have been found to live in X-ray selected COSMOS groups (George et al. 2011). No group catalogs are available at higher redshift.

In Figure 5 the same quantities for data drawn from the models are also overplotted. The upper panel shows the results for the DLB07 model, the lower panel for the H15 model. At each redshift, we randomly extract the same number of progenitors found in observations at the corresponding redshift, and then we compute the projected distances to define the number of companions within a certain projected radius.[9] We repeat the sampling 10 times, to take into account sample variance. We then consider the maximum range spanned by the extractions. Qualitatively, within a large spread, both the DLB07 and H15 models follow the observational trends at all distances. Nonetheless, there are extractions where the number of galaxies is systematically higher than observed in both models and at all distances, especially in the DLB07 one. This might be related to the well known issue of the over-prediction of the number of satellites (e.g., Fontanot et al. 2009; Weinmann et al. 2011) and has also been found to be present in clusters (Vulcani et al. 2014). Discrepancies are solved by construction in the H15 model.

The fact that in simulations there is a non-negligible spread among the different extractions indicates that the sample variance is not marginal, therefore a larger sample of observed galaxies will be needed to draw more robust conclusions.

[9] For each galaxy we consider projected distances on the *xy*, *xz,* and *yz* planes.

Our results are in line with the results of Tal et al. (2013), who found that the total number of galaxies within a mass range of 1:10 and within roughly 400 kpc of the massive galaxy is on average two to three in all redshift bins (see also Quilis & Trujillo 2012; Tal et al. 2012; Gobat et al. 2015).

5.2. Comparisons with the Stellar Mass Function

To further assess the environment in which the observed progenitors live, we estimate how many satellites progenitors should have, based on the stellar mass function down to 1:10 the mass of the progenitor. This number could give us hints as to whether most of them live in clusters/groups or in the field.

Tal et al. (2014) presented the stellar mass function of satellites around the central galaxies of different stellar masses at $0.2 < z < 1.2$. They identified central galaxy candidates from the UltraVISTA catalog. Galaxies were considered to be central if no other more massive galaxies could be found within two projected virial radii. Virial radius estimates at a given stellar mass and redshift were determined using the semi-analytic model of Guo et al. (2011). They found that the mass distribution of satellite galaxies is independent of redshift for any given value of central galaxy mass. If we hypothesize that our progenitors are the central galaxies of a group, we can integrate the Tal et al. (2014) mass function from the mass of the progenitor down to 1:10 of its mass, and compare the expected number to our observed ones. Analytically, we find that we should expect two to three companions per central galaxy within two projected virial radii.[10] Following Muñoz-Cuartas et al. (2011), at $z \sim 1$, the typical virial radius of haloes with $M_{\rm vir} \sim 10^{13}\ M_{\odot}$ is $\sim$0.5 Mpc. If we therefore consider a radius of 1 Mpc, we find that for $z > 1$ 15% of the progenitors have at most one companion, while for $z < 1$ there are no isolated progenitors. This might suggest that most progenitors live in massive structures like groups or clusters, but at least at high redshift there is a non-negligible fraction that have no companion.

At $z < 1$ we can push down the mass limit to 1:100 without being biased by mass-incompleteness. With this mass threshold, analytically, we should expect around nine companions per central galaxy within two projected virial radii. In our observations we find an average of 50 ± 5 galaxies within the same radius. This might suggest that at least our low-redshift progenitors are located within structures that are largely dominated by the presence of small galaxies. As we will see in Section 6.3, even though there is not much mass enclosed in these galaxies, they play a role in the mass growth of the progenitors given their high Specific Star-Formation Rate (sSFR).

5.3. Number of Satellites as a Function of Distance

We now focus our attention on progenitors with at least one companion within 500 kpc and investigate, on average, the variation of the number of companions per projected volume with distance, both in observations and in models (Figure 6). In observations, trends with redshift are not detected. However, if we sum up the number of companions, we find 4.6 ± 0.9, 4.8 ± 0.5, 3.7 ± 0.3, and 3.6 ± 0.3 galaxies within 500 kpc per progenitor from $0.2 < z < 0.5$ to $1.5 < z < 2$, respectively. Trends with distance are also detected. The number of companions drops between distances of 100 and 200 kpc and is nearly constant at larger distances.

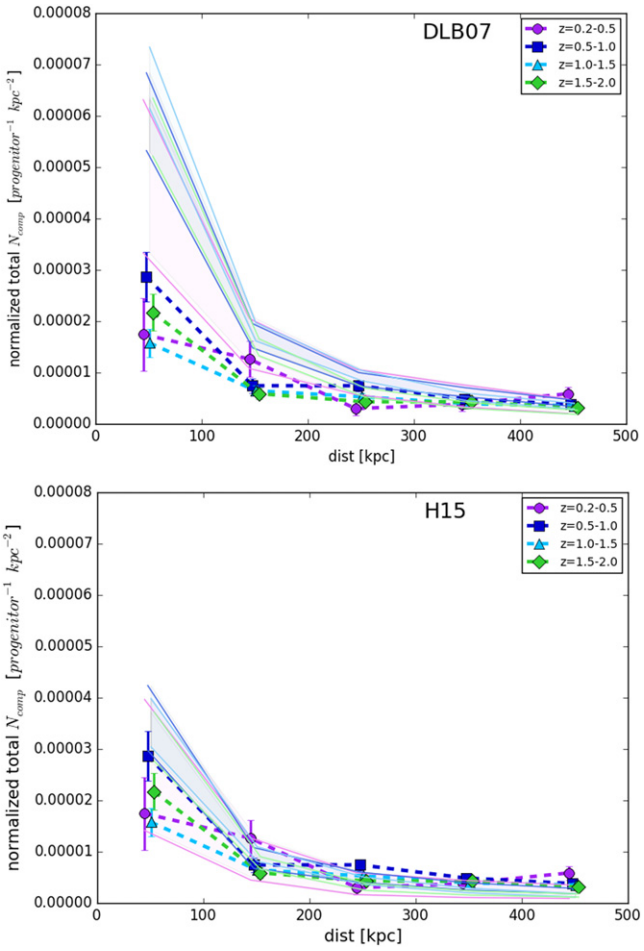

Figure 6. Number of companions per progenitor per kpc^2 as a function of distance at different redshifts, as indicated in the labels. Only progenitors with at least one companion within 500 kpc and galaxies at least as massive as 1:10 the mass of the progenitor and with z within $\pm 0.05 \times (1 + z_{\rm pr})$ are considered. Errors are poissonian. A horizontal shift is applied to the points for the sake of clarity. Thick dashed lines and points represent observations; thin solid lines and shaded areas represent models (upper panel: DLB07, bottom panel: H15). In models, error bars represent the range spanned by the 10 extractions.

Models show stronger trends with distance. In the DLB07 model (upper panel of Figure 6) there is on average a larger number of companions around each progenitor than in observations, especially at small distances (<100 kpc) where the number of galaxies is more than a factor of two larger than in observations. Considering 10 different random extractions, the median number of galaxies around progenitors within 500 kpc is 6 ± 1, 7.4 ± 0.5, 7.3 ± 0.4, and 5.9 ± 0.3 from $z = 0.36$ to $z = 1.77$, respectively. This again might be due to the over-prediction of the number of satellites in the DLB07 prescription. By contrast, in H15 (bottom panel of Figure 6), the number of objects is typically consistent with the observed (median numbers are 3.5 ± 0.8, 3.7 ± 0.4, 3.6 ± 0.3, and 3.1 ± 0.2). In both models, no trends with redshift are detected, even though the DLB07 model shows a possible inversion in the lowest redshift bin.

Our findings are consistent with the idea that progenitors are centrals (i.e., surrounded by a satellite population with some decreasing number density profile). Indeed, as shown in

[10] Two virial radii is the size chosen by Tal et al. (2014).

Table 1, in both models and at all redshifts >90% of the selected galaxies are classified as centrals in their haloes.

The discrepancies found in the DLB07 model are noticeably alleviated if we exclude type 2 galaxies (plots not shown), which are mostly found at close distances from the center of the haloes. Similarly, also in the H15 model, the number of galaxies at ∼50 kpc is strongly reduced when type 2 galaxies are removed. We note, however, that type 2 galaxies cannot be excluded: it has been shown that their presence is fundamental to reproduce several properties (i.e., the clustering at small scales of the structures and the differences between the galaxy and subhalo profiles in the inner regions of clusters; Gao et al. 2004; Wang et al. 2006).

We can also investigate whether progenitors with different star-forming properties live in different environments. Models do not provide us with the necessary information to distinguish between star-forming and quiescent galaxies as was done for observations; nonetheless, for both models and observations, we can use the galaxy sSFR (= SFR/M_*) to distinguish between star-forming and quiescent galaxies. We assume that galaxies with log sSFR < -11 are quiescent, this being the minimum of the distribution. In observations, this number roughly corresponds to the adopted $U - V$ versus $V - J$ cut.

In observations, as already mentioned, while at $z < 1$ all progenitors are quiescent, at higher redshift 60% of progenitors are star forming. In addition, in models the fraction of quiescent galaxies depends on redshift, spanning from ∼95(78)% to ∼30 (17)% in the DLB07 (H15) model going from low to high-z. Both in observations and simulations there is no significant difference in the trends shown in Figure 6 when we select only quiescent candidate progenitors.

Similarly, we now focus on the properties of the companions, checking whether the distribution around progenitors depends on their star-forming properties. Figure 7 shows the variation with distance and redshift of the number of quiescent galaxies around quiescent progenitors both in observations and simulations. Trends resemble those found for the total population. In observations, the distance dependence is less steep, whereas in models there are hints it might be steeper. Both models show an over abundance of satellites at small distances. Because the overall the trends are similar in Figures 6 and 7, we can conclude that there are no evident signs of clustering in observations, where the quiescent and star-forming galaxies are similarly distributed around progenitors, whereas in models it seems that quiescent galaxies might be more clustered around quiescent progenitors. In observations, similar results have been obtained when using a $U - V$ versus $V - J$ cut, showing that the results are not very sensitive to the cut adopted to separate star-forming from quiescent galaxies.

To summarize, we found that the number of companions around progenitors does not depend on redshift. In observations, going from higher to lower redshift and from smaller to larger distances, the environment gets proportionally richer in galaxies. Nonetheless, there is a fraction of progenitors that do not have companions, suggesting that their mass growth is unlikely related to merger events. Excluding isolated progenitors, we found that the distribution of companions per projected volume is almost independent of redshift.

In models, the fraction of isolated progenitors is much lower, indicating that progenitors live in denser environments.

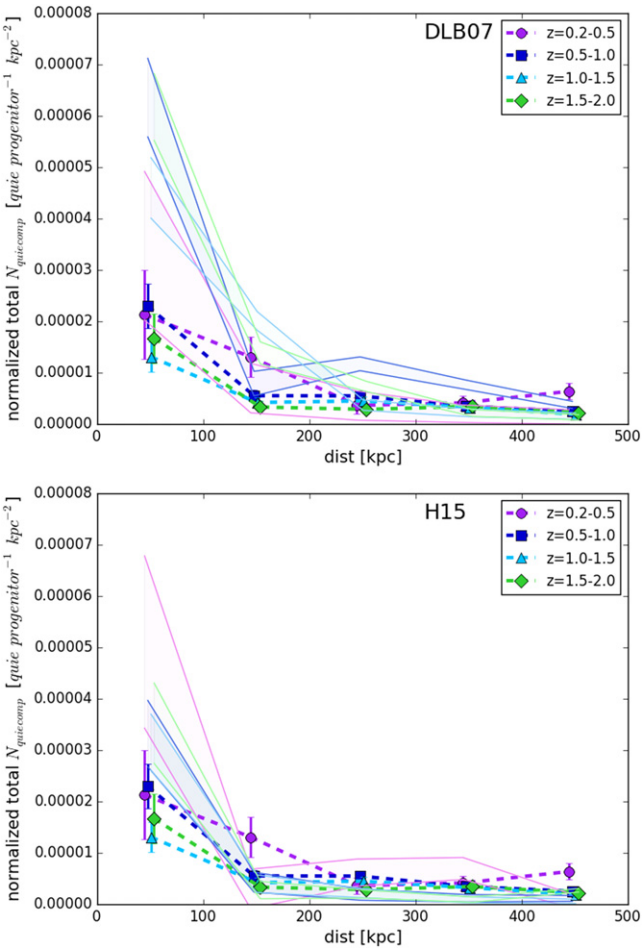

Figure 7. Number of quiescent companions per quiescent progenitor per kpc^2 as a function of distance at different redshifts, as indicated in the labels. Points, lines, error bars, and colors are as in Figure 6.

6. THE DRIVERS OF THE PROGENITORS' MASS GROWTH

In this section we aim to investigate which are the most important factors that drive the galaxy mass growth for progenitors from $z \sim 2$ to $z \sim 0$. We will first focus only on mergers (Section 6.1), then we will quantify the contribution of in situ star formation (Section 6.2), and finally we combine the two (Section 6.3) to estimate their relative importance at the different redshifts.

6.1. What Fraction of Galaxy Mass Growth is Due to Mergers?

Kitzbichler & White (2008) investigated the major merger rates using catalogs based on the DLB07 model to obtain the characteristic timescale needed by two galaxies of a given mass ratio and redshift to merge on the basis of their projected distance. In the model, to determine whether or not two galaxies might merge, it is assumed that when the subhalo that hosts a galaxy is tidally disrupted near the center of a more massive halo, the galaxy becomes eligible to merge with the central galaxy of that halo. Nonetheless, the merger does not occur immediately, but rather after a "dynamical friction time"

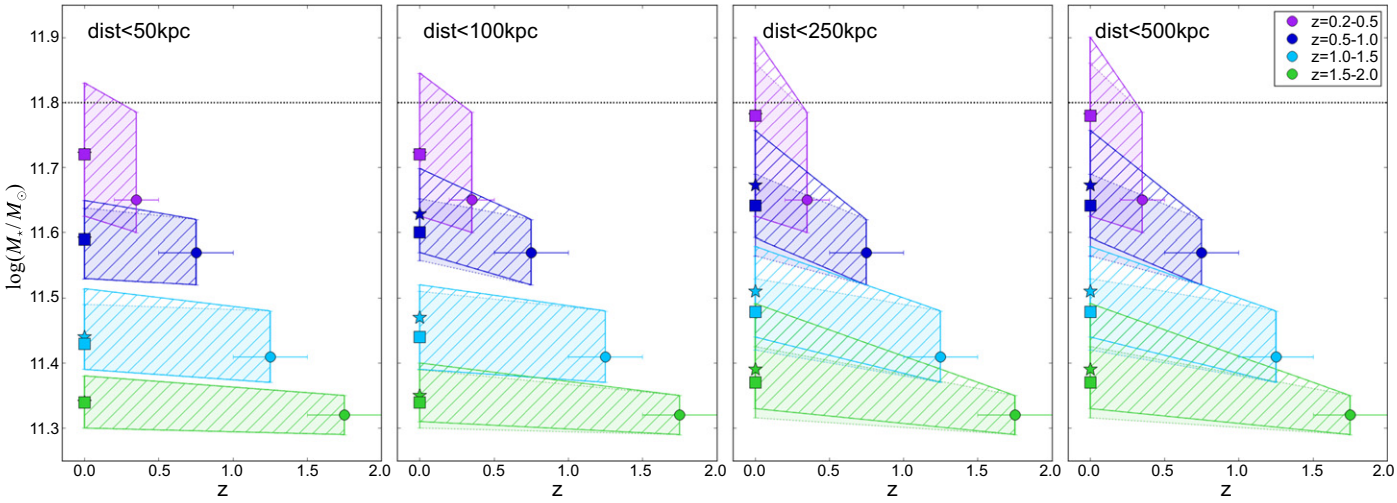

Figure 8. Observed median progenitor mass growth at different redshifts, as indicated in the labels, assuming that galaxies within 50, 100, 250, and 500 kpc will merge by $z = 0$ onto the progenitor. The mass at $z = 0$ is the sum of the entire mass (stars and dashed regions) or half the mass (squares and shaded regions) of all galaxies with mass ratio 1:10 and redshift ± 0.1. Error bars on the x-axis represent the width of the redshift bin; error bars on the y-axis represent the 25th and 75th percentiles. The dotted horizontal lines represent the mass of the UMGs at $z \sim 0$ (from Marchesini et al. 2014).

estimated from the relative orbit of the two objects at the moment of subhalo disruption.

For $z \leqslant 1$, stellar masses above $5 \times 10^9 M_\odot$ and samples limited to radial velocity difference $\Delta v < 3000\,\mathrm{km\,s^{-1}}$,[11]

$$\left\langle T_{\mathrm{merge}} \right\rangle = 3.2\ \mathrm{Gyr} \frac{r_p}{50\ \mathrm{kpc}} \left(\frac{M_*}{4.6 \cdot 10^{10} M_\odot} \right)^{-0.3} \left(1 + \frac{z}{20} \right), \quad (1)$$

where T_{merge} is the timescale, r_p the projected physical separation, M_* the stellar mass of the pairs, and z the redshift of the progenitor.

Kitzbichler & White (2008) do not provide a formula for higher redshift galaxies, therefore we use the same parametrization at $1 < z < 2$. Given the range of masses and redshifts in our sample, we find that galaxies located more than ~350 kpc apart at $z \sim 2$ should not go through a merger event by $z = 0$.

We can therefore estimate the mass growth due to mergers by summing the stellar mass in companion galaxies that are expected to merge by $z = 0$ with the mass of the progenitor.[12] We analyze two cases: in the first, we assume that the entire mass in the companions will end up in the mass of the progenitor, in the second case, only half of it will and the other half is assumed to go into some diffuse component. These are two extreme cases that should bracket the real situation (e.g., Conroy et al. 2007; Lidman et al. 2013; Burke et al. 2015).

Figure 8 shows the median mass growth that observed progenitors are expected to have from their redshift to $z \sim 0$.[13] In the local universe, the typical stellar mass of UMGs is $M_\star \sim 10^{11.8}\ M_\odot$ (Marchesini et al. 2014).

We consider different bins of distance, and therefore only galaxies within a certain distance from the progenitor. Going to very large distances allows us to be as inclusive as possible in terms of companions to count and give an estimate of how much the mass growth changes as a function of distance.

First, we note that the dispersion (described as the 25th and 75th percentile of the distributions) around the median mass is asymmetric and is mainly due to the fact that we are on the exponential tail of the mass function, therefore distributions are not normal.

The figure shows that the mass growth depends on the considered distance. Taking into account only galaxies within 50 kpc from the progenitor, the mass growth is negligible for galaxies at $z > 0.5$. By contrast, mergers alone might explain the growth of galaxies from $0.2 < z < 0.5$ to $z = 0$. Increasing the radius of interest, the mass growth due to mergers increases; nonetheless, it is generally still insufficient to justify the expected mass growth. This is true assuming that the entire mass in the companions will end up in the mass of the progenitor, or that only half of it will.

Taking into account all galaxies that can actually merge with the progenitor from their redshift to $z = 0$, on average, galaxies increase their mass of $41 \pm 9\%$, $33 \pm 1\%$, $27.9 \pm 0.4\%$, and $31.4 \pm 0.6\%$ from $z \sim 0.35$, 0.75, 1.25, and 1.75, respectively.

We note that only for $z < 1$ can we include in the computation galaxies with smaller mass ratio (down to 1:100) with respect to the mass of the progenitor, without being affected by sample incompleteness. Considering these galaxies in the computation does not strongly influence the results (plots not shown), simply because despite there being many more galaxies, their low-mass is negligible with respect to the mass of the progenitor.

When inspecting models (Figure 9), similar results are obtained for the lowest redshift bin and the mass growth for galaxies at $z = 0.36$ is compatible with the mass of the local UMGs. In addition, the DLB07 model can explain the mass growth in terms of mergers from $z = 0.76$ (1.28) to $z = 0$ when a radius $\geqslant$100 (250) kpc is considered; the H15 model can explain it when a radius $\geqslant$250 kpc is considered. We

[11] The authors suggest using the timescales for $\Delta v < 3000\,\mathrm{km\,s^{-1}}$ when analyzing data from photometric redshift samples, because the "background" correction will not eliminate physically associated galaxies at large velocity separation.

[12] For each pair progenitor-companion we estimate the time they need to merge and evaluate if they will merge, eventually.

[13] We note that our values slightly differ from those presented in Marchesini et al. (2014) because they adopt mean masses, whereas we use median values.

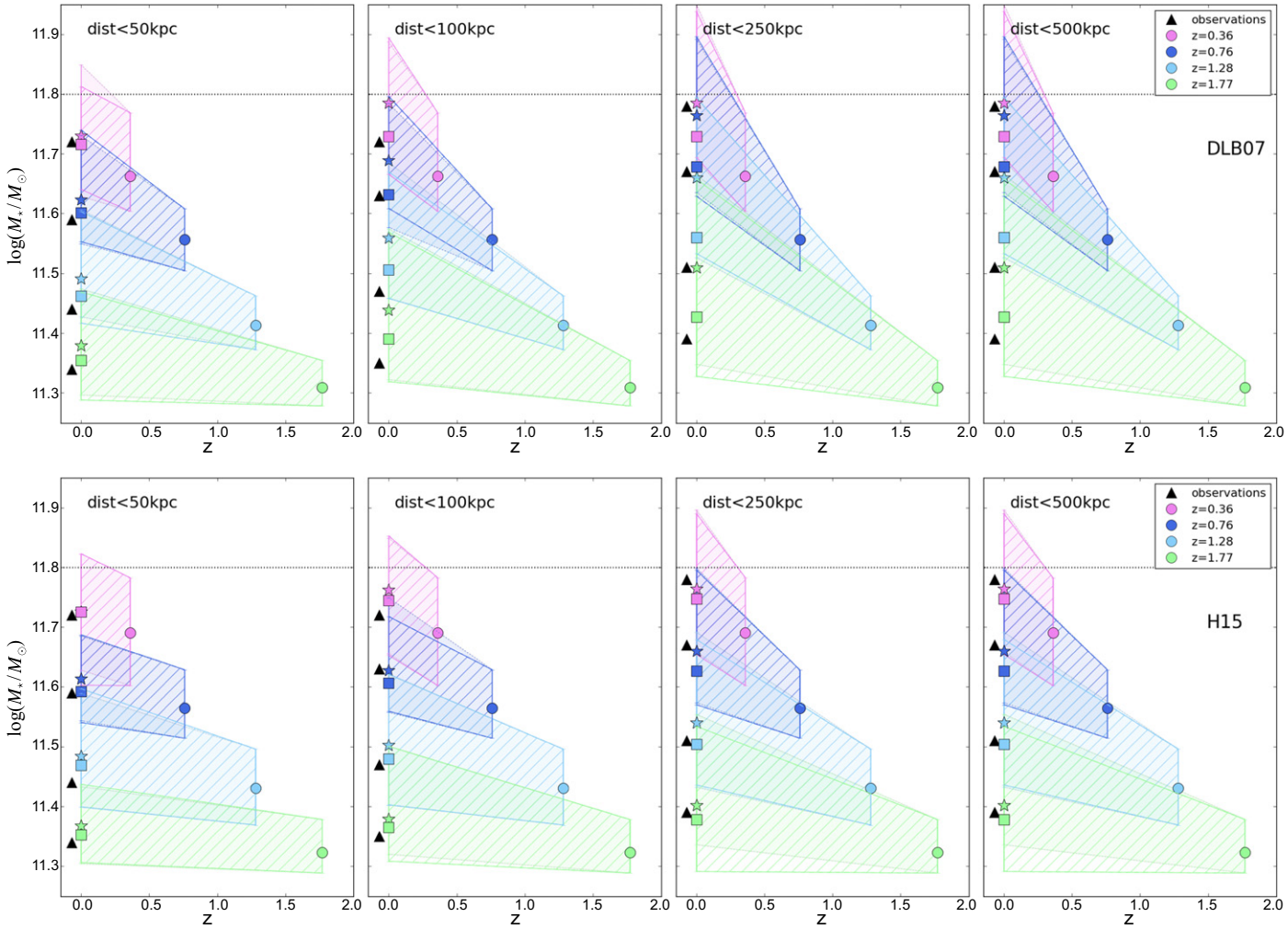

Figure 9. Predicted median progenitor mass growth at different redshifts, as indicated in the labels, assuming that galaxies within 50, 100, 250, and 500 kpc will merge by $z = 0$ onto the UMG. The mass at $z = 0$ is the sum of the entire mass (stars and dashed regions) or half the mass (squares and shaded regions) of all galaxies with mass ratio 1:10. Error bars on the y-axis represent the maximum the 25th and 75th percentiles of the 10 representations. Upper panel: DLB07, bottom panel: H15. The dotted horizontal lines represent the mass of the UMGs at $z \sim 0$ (from Marchesini et al. 2014). Black triangles represent the inferred mass at $z = 0$ from observations, assuming that all the mass of the satellites falls into the progenitor.

emphasize the large spread that characterizes the models, which indicates the variety of growth histories that characterizes galaxies.

Recall that in the left panel of Figure 2, where we compared the stellar mass of the progenitors and their descendants as given by the models, we found that in the H15 model the mass growth is such that the descendants at $z = 0$ do not have a mass of $\sim 10^{11.8}\ M_{\odot}$, indicating that in this model the progenitor selection did not work properly. This is due to the fact that in the H15 model not all mass in the merging galaxies ends up in the central one, but a non-negligible fraction goes into the intracluster medium (H15).

In summary, this analysis suggests that mergers alone can only explain the mass growth of the progenitors of the local UMGs for galaxies at $z < 0.5$ in observations, and $z < 1$ in simulations. By contrast, they do not produce enough mass for galaxies at higher redshift. This is due to the fact that at $z > 1$ progenitors are isolated or have very low-mass companions, whose mass is not sufficient to explain the expected trends. These results suggest that other factors may play an important role in the galaxy mass growth.

6.2. *What Fraction of Galaxy Mass Growth is Due to Star Formation?*

Figure 10 shows the amount of mass that progenitors are expected to gain for star formation, both in observations and models. In observations, we adopt both the SFR estimates obtained from the SED fitting and those obtained from the UV+IR. The latter are systematically higher than those obtained from the SED fitting and give us an upper limit of the growth. In simulations, we use the SFR estimates provided by the two semi-analytic models.

We consider a constant SFR in the range of time between the redshift of the galaxy and the lowest limit of the next redshift bin. In this way, our estimates most likely represent an upper limit of the real situation.[14] In the computation, we take into account the fact that the stellar mass of a galaxy changes with time and also simply due to the evolution of its stars: as they progressively evolve and eventually die, they retain only part of their mass as remnant. Following Poggianti et al. (2013), who

[14] In observations, considering a declining SFR does not strongly change the results (plots not shown).

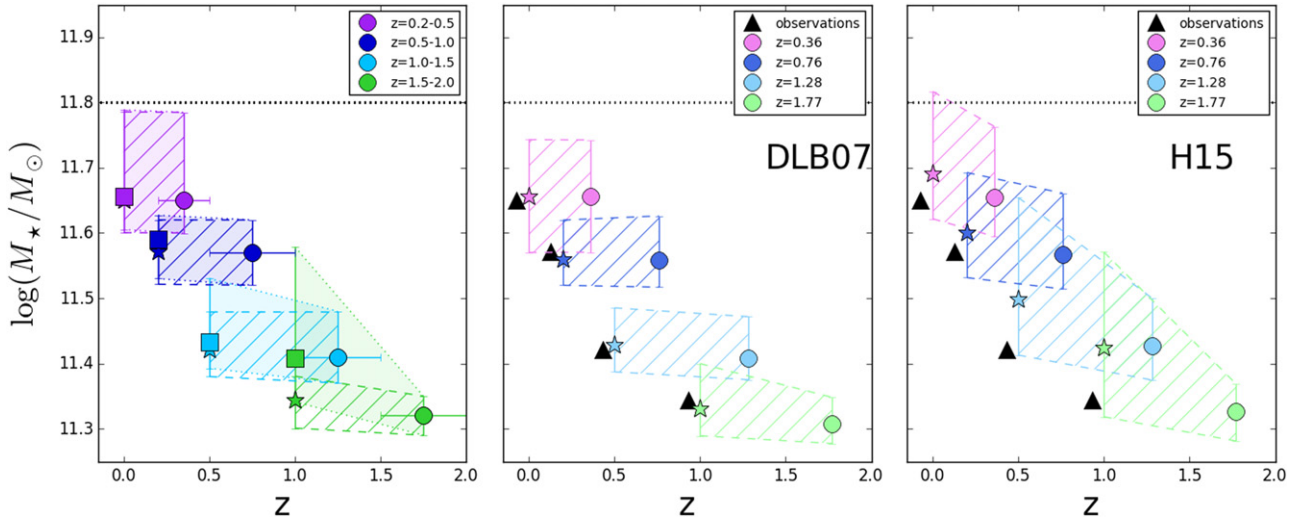

Figure 10. Median progenitor mass growth due to a constant star formation at different redshifts, as indicated in the labels. Left panel: observations. Stars and dashed regions show the mass growth adopting SFR estimates from SED fitting; squares and shaded regions show the mass growth adopting SFR estimates from UV+IR. Central panel: DLB07 model, right panel: H15 model. In the panels showing the models, black triangles represent the values obtained from observations. Error bars on the *x*-axis represent the width of the redshift bin (only in observations), error bars on the *y*-axis represent the 25th and 75th percentiles.

used the Bruzual & Charlot (2003) model, the fraction of the initial stellar mass that remains is equal to 1 for ages less than 1.9×10^6 year, whereas it can be approximated as $f(t) = 1.749 - 0.124 \times \log t$ at older ages, where t is the age of the stellar population in years. Approximately, in 0.6 Gyr galaxies retain ∼60%–70% of the mass they have formed.

The left panel of Figure 10 shows the results for the observations. Estimates from SED fitting produce a little mass growth, while estimates from UV+IR can explain the mass growth from one redshift bin to the next. In the DLB07 model (central panel of Figure 10) the median values obtained are comparable to those observed from SFR estimated from the SED fitting. As in observations, star formation alone can only marginally explain the mass growth. In addition, results of the 10 different extractions are quite similar, as indicated by the moderately small scatter. This suggests that in the DLB07 model, galaxies of similar mass have similar SFR at the time they have been selected. In contrast, values in the H15 model (right panel) are systematically larger than the observed ones, even though there are some extractions where they show agreement. Note that in the H15 model, the scatter is very large, indicating that galaxies of similar mass can have a wide range of SFRs.

6.3. Combining the Contribution of SFR and Mergers

In the previous subsections we found that neither mergers nor star formation alone are able to fully explain the expected progenitors' mass growth from $z = 2$ to $z = 0$, both in observations and, to some extent, in simulations. Here we aim to test whether the combined contribution of in situ and environmental processes can produce the expected growth. We also consider the mass growth due to star formation in the galaxies that will merge with the progenitors. We note that our analysis does not consider the contribution from a starburst during mergers. This is probably not a dominant channel for mass growth, but it might play a somewhat more important role at higher redshift.

As in the previous section, we compute the mass growth due to star formation in the time interval between the redshift of the galaxy and the next redshift bin. In this case we use the same time interval to estimate the contribution of mergers so that we can sum them up together. The left panel of Figure 11 shows the results for the observations. Considering all galaxies that might eventually merge, when the SFR determined from the SED fitting is adopted, the combination of the two contributions marginally explains the mass growth, barely tracing the lower limit of the growth. Instead, when we adopt the SFR estimates obtained from the combination of UV and IR luminosities, we recover the expected mass growth. Recall that the $\mathrm{SFR_{UV+IR}}$ represents an upper limit of the true values, given that at these redshifts the AGN contamination might not be negligible. However, the SFR estimated from the UV+IR is arguably less biased against heavily obscured star formation. Therefore, the real growth is expected to be bracketed between these two cases.

The central and right panels of the same Figure show the results for the two semi-analytic models. Both predict a growth that is sufficient to support the expected mass growth at all redshifts. Again, the large scatter that characterizes the models suggests that the different extractions we performed from the catalogs can give quite different results.

The results obtained in the right panel for the H15 model are in disagreement with the results presented for the same model in Figure 2. When we apply the same prescriptions in the observations to account for the growth from both merging and in situ star formation from one redshift bin to the following one, the inferred mass is in agreement with the mass of the progenitors at that redshift. As a consequence, we can grow all progenitors to a mass of $\sim 10^{11.8}\ M_\odot$ at $z = 0$. In contrast, when we directly consider the mass of the descendants at $z = 0$ as provided by the models, we find a systematically smaller mass for the galaxies of the same initial mass. This means that some of the assumptions made to estimate these contributions may not be sufficient or may be incorrect (e.g., stripping and/or merger rates) when adopted for this particular model, as will be discussed in the following section.

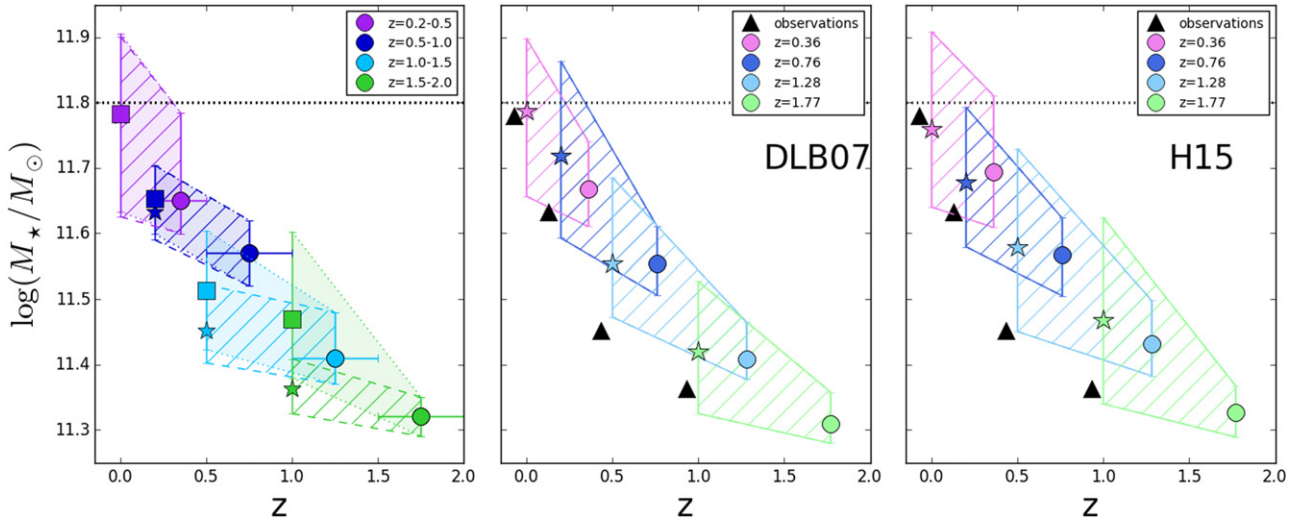

Figure 11. Median progenitor mass growth due to both star formation and merger at different redshifts, as indicated in the labels. The satellites' mass growth is taken into account. A constant SFR and the assumption has been made that the mass of the satellites will end up within the mass of the progenitor. Left panel: observations. Stars and dashed regions show the mass growth adopting SFR estimates from SED fitting; squares and shaded regions show the mass growth adopting SFR estimates from UV+IR, central panel: DLB07 model, right panel: H15 model. In simulations, black triangles represent the values obtained from observations. Error bars on the *x*-axis represent the width of the redshift bin (only in observations), error bars on the *y*-axis represent the 25th and 75th percentiles.

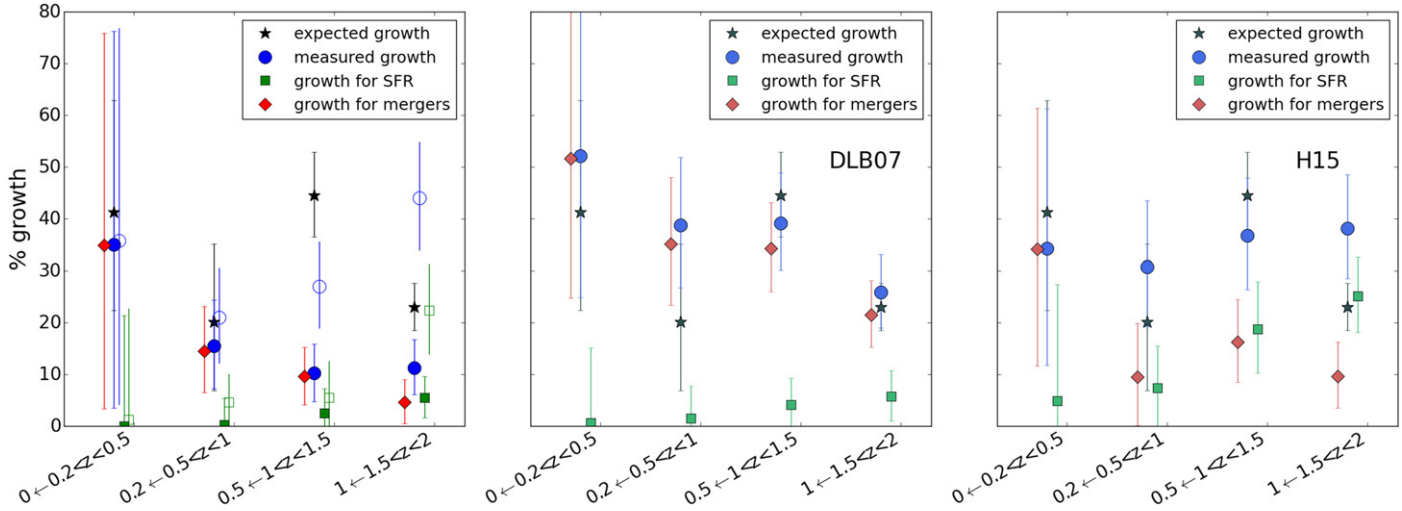

Figure 12. Percentage of the mass growth as a function of time as expected by the abundance matching technique (black stars); as measured considering the combined contribution of SFR, mergers and SFR in the satellites that will merge (blue points); as measured considering only SFR in the progenitors (green squares) and only mergers (red diamonds); for observations (left panel), the DLB07 model (central panel), and the H15 model (right panel). In observations, values were obtained both considering the SFRs from the SED fitting (filled circles) and those from the UV+IR (empty circles). A shift has been applied to the points for the sake of clearness. Error bars represent the maximum and minimum growth, which were obtained propagating the errors on the medians (Rider 1960).

7. DISCUSSION

The main results of our analysis are summarized in Figures 12 and 13. The former presents the relative contribution of star formation and mergers to the mass growth, showing the inverse of ratio of the progenitor stellar mass at a given redshift to the inferred stellar mass at the same redshift. The expected stellar mass growth from the abundance matching technique, the total measured stellar mass growth obtained considering mergers and star formation, and the separate contribution of star formation and mergers are shown. The latter figure shows the cumulative mass growth due to the two contributions, separately. In both figures, the quoted uncertainties represent the maximum and minimum growth, while errors on the medians are estimated as $1.253\sigma/\sqrt{N}$, where σ is the standard deviation about the median and N is the number of galaxies (Rider 1960).

In observations (left panels) the total mass growth we obtained is below the expectations when the SFR values are obtained from the SED fitting. Trends are driven by high-z galaxies: from $1 < z < 1.5$ to $z \sim 0.5$ we measure a growth of $\sim$10% while the expected growth is $\sim$40%. This entails that at $z = 0$ $\sim$20% of mass is lacking. In contrast, discrepancies are largely reduced when SFRs are measured from a combination of UV and IR luminosities. In this case, the inferred mass growth is even larger than the expected one at the highest redshift.

Focusing on models (central and right panels), both prescriptions are able to fully explain the mass growth as predicted by the abundance matching technique, and, possibly, even overpredict it.

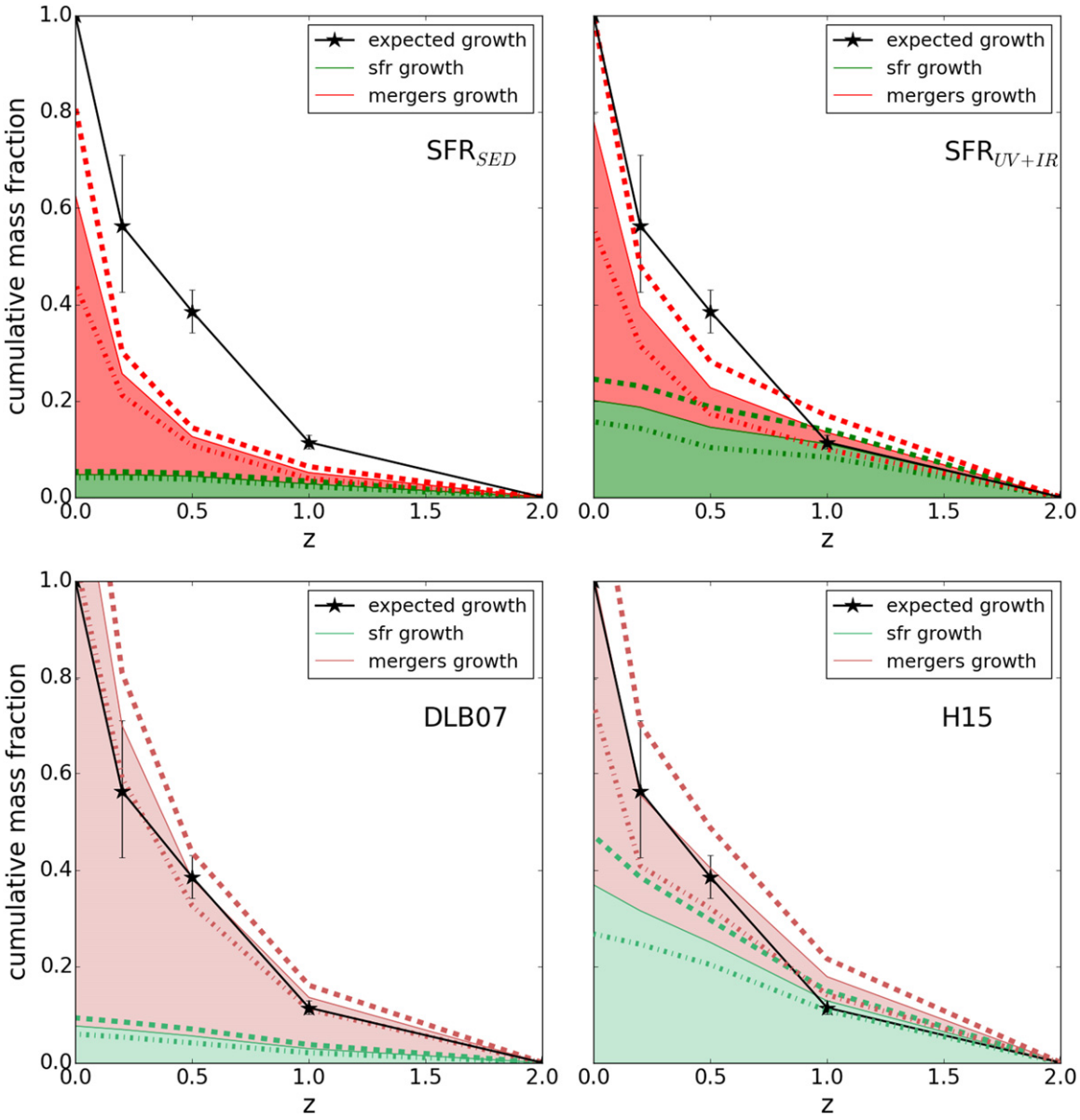

Figure 13. Mass build-up over time due to star formation and mergers. Upper panels: observations; left panel: SFR from the SED fitting, right panel: SFR from the UV +IR luminosities. Bottom panels: simulations; left panel: DLB07, right panel: H15. Black stars and solid lines represent the expected mass growth from Marchesini et al. (2014) with the uncertainties; red regions represent the contribution of mergers to the mass growth and green regions represent the contribution of SFR to the mass growth. Thick dashed lines represent the upper limit of the contributions, while thick dashed–dotted line represents the lower limit, and both are obtained propagating the errors on the medians (Rider 1960).

Investigating separately the contribution of star formation and mergers, we find that they play a very different role at the different redshifts. In observations, the average SFR is similar to the net growth rate at $z = 1.5$–2, but significantly smaller at later times. The progenitor's star formation is only important at the highest redshifts, where it might be able to soley explain all the mass growth. At lower redshifts, mergers acquire importance and are the major cause of the observed evolution at $z < 0.5$. At the intermediate redshifts, the growth can be explained by advocating the combined contribution of star formation and mergers.

Overall, these findings are in line with many other studies (e.g., van Dokkum et al. 1999, 2010; Tran et al. 2005; van Dokkum 2005; Bell et al. 2006; Naab et al. 2007, 2009; White et al. 2007; McIntosh et al. 2008; Ownsworth et al. 2014), even though some works have suggested that major mergers may play a more prominent role with up to ∼60% of a massive galaxy's stellar mass growth at $z < 2$ arising from major merger events (e.g., López-Sanjuan et al. 2012; Ferreras et al. 2014; Ruiz et al. 2014).

In both models, the contribution of star formation to the total mass growth decreases with time. However, it plays a larger role in the H15 model than in the DLB07 at all redshifts, and it shows a steeper decline with time. It goes from 20% to 5% in the H15 model and from <10% to 0% in the DLB07 model. In the DLB07 model the contribution of mergers increases with time, ranging from 20% to 50%, with a slope that is similar to the observed one. However, contrary to observations, they are much more important than star formation, even at higher redshift. In contrast, in the H15 model the contribution of

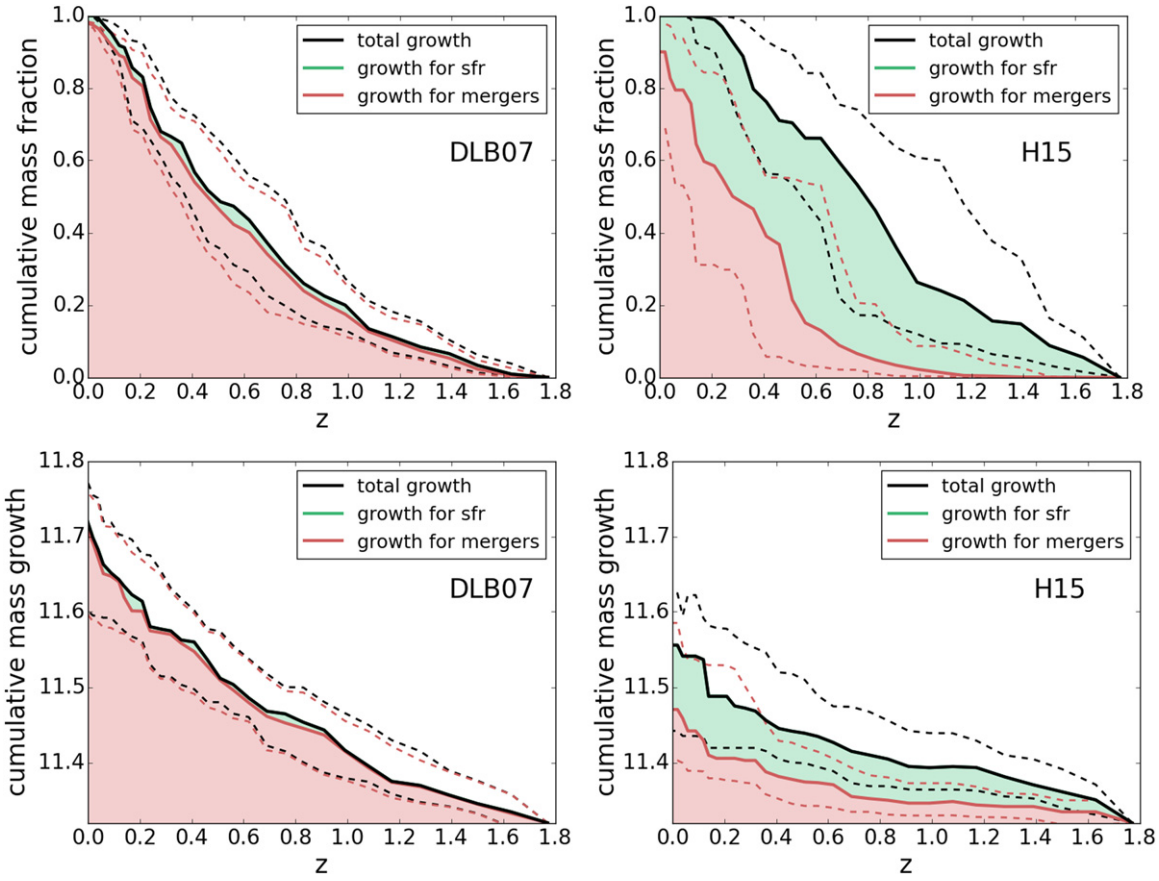

Figure 14. Predicted mass build-up over time due to star formation and mergers, as obtained from the merger trees for the DLB (left panels) and H15 (right panels) models. Upper panels: cumulative mass fraction, lower panels: cumulative mass growth. The median of 70 merger trees is shown (solid lines), along with 1σ dispersion (dashed lines). Black lines: total growth, red lines and areas: growth due to mergers, green lines and areas: growth due to star formation. See text for details.

mergers is roughly constant with time, showing a bump only in the lowest redshift bin. Values are similar to the observed ones.

As already mentioned, the non-negligible spread measured among the different extractions in simulations indicates that the sample variance is not marginal, therefore a larger sample of observed galaxies will be needed to draw more robust conclusions.

In models, we can explicitly investigate the separate role of mergers and star formation by inspecting the merger trees of a subsample of galaxies in the highest redshift bin. We consider only progenitors at $z = 1.77$, because most of the progenitors at lower redshift are actually descendants of these galaxies, and therefore will enter their merger trees later on.

In both models, for each progenitor we select all the galaxies in the merger tree that have the same direct descendant in the next snapshot and we sum up the masses of the merging galaxies to compute the mass growth due to mergers. We then compare the mass of the merged galaxies to the mass of their unique descendant and assume that the difference is due to star formation.[15] Note that in the H15 model we consider only the galaxies that actually merged, and not those that were disrupted before merging onto its descendant, whose matter went into the intracluster medium. We then start from the descendant and repeat the loop down to $z = 0$, in order to trace the entire growth.

Figure 14 shows the median relative mass growth and the median total mass growth for 70 galaxies[16] in the DLB07 and H15 models, respectively. As found in the previous sections, the contribution of mergers and star formation is different in the two prescriptions, with mergers relatively more important in the DLB07 model than in the H15 one. In H15, star formation also plays an important role at low redshift. Most importantly, we find that in the two models, galaxies are characterized by an overall very different mass growth. In line with the results shown in Figure 2, from $z = 1.77$ to $z = 0$ galaxies in the DLB07 model grow $\times 1.5$ more than in the H15 model. This is likely due to the modifications in the H15 model, which add the tidal stripping and reduce the mass of the merging satellites, therefore producing a smaller mass growth. Nonetheless, this result is quite surprising given the fact that the model reproduces the evolution of the stellar mass function and has been calibrated to be in better agreement with the halo occupation distribution results (H15), which the abundance matching technique relies on. Understanding the reasons of these discrepancies is beyond the scope of this paper, and is deferred to a forthcoming work.

7.1. Some Caveats

Overall, our analysis reveals some tensions between the mass growth expected by the abundance matching technique and the mass growth measured taking into account in situ star

[15] Note that this means the stars formed during starbursts associated with mergers are going to be in the mass growth phase.

[16] This is the number of the observed progenitors at $1.5 < z < 2$.

formation and mergers, both in simulations and in observations. The largest discrepancy is seen between $1 < z < 1.5$ and $0.5 < z < 1$ in observations, when the SFRs from the SED fitting are used. We note that these two contiguous redshift bins bracket a break in the galaxy property distribution: at $z > 1$ many progenitors and satellites are still star forming, whereas at $z < 1$ all the progenitors and most of the satellites are quiescent (see also Marchesini et al. 2014). As we will see later on, this transition regime might be responsible for this gap.

Overall, discrepancies might be due to a number of factors. First, it might be that the abundance matching technique adopted to link galaxies across time does not work properly. However, our analysis shows that candidates are selected well, at least for DLB07 model. Quite surprisingly, the H15 does not support the selection via the abundance matching technique. Indeed, the mass growth estimated for the H15 model and the one that is intrinsic in the model (as shown in Figures 2 and 13) are not in agreement. Understanding the weakness of the selection criteria is beyond the scope of this paper, since the method has been largely discussed in the literature and it has been found to provide an excellent match to a number of galaxy clustering statistics at multiple epochs (Kravtsov et al. 2004; Tasitsiomi et al. 2004; Vale & Ostriker 2004, 2006; Berrier et al. 2006; Conroy et al. 2006; Marín et al. 2008; Trujillo-Gomez et al. 2011) and to a number of population properties (e.g., Drory & Alvarez 2008; Conroy & Wechsler 2009).

Alternatively, discrepancies might be due to some assumptions made. For example, it might be that in reality mergers play a less important role at higher redshift than that estimated by Kitzbichler & White (2008) at $z < 1$. Even though merger rates are not expected to vary much with redshift (e.g., Guo & White 2008; Kitzbichler & White 2008; Wetzel et al. 2009), we might be overestimating the number of mergers.

In addition, in our treatment we are not considering some other factors that indeed might play a role. The most important is the contribution of galaxies whose mass is lower that 1:10 the mass of the progenitor and therefore do not enter our selection. These galaxies can be characterized by high sSFR values, hence they double their mass rapidly, therefore giving a non-negligible contribution to the total growth. We checked that at least at $z < 1$, where our sample is not affected by incompleteness, including in the computation all galaxies with a mass ratio of 1:100 to better reconcile the expected to the observed growth (plot not shown). We cannot extend to higher redshift because of incompleteness effects. We note, however, that at $z > 1$ the contribution of satellites with mass ratio larger than 1:10 might play a more important role than that at lower redshift. Indeed, most of them are star forming and are probably characterized by high sSFR values, therefore giving a large contribution to the total growth. At $z < 1$ many satellites are quiescent and contribute less to the total growth.

Additionally, mergers can also induce bursty events of star formation, which can pump up galaxy masses. However, it is very hard to properly model these bursts and quantify their role in the overall galaxy growth. Not considering the contribution from starburst during mergers have a larger impact at $z > 1$ that at $z < 1$. Indeed, at higher redshift mergers most likely involve star-forming galaxies and are accompanied by bursts that enhance galaxy star formation with a consequent larger mass growth, whereas at lower redshift mergers most likely take place between quiescent galaxies, therefore bursts are rare.

Finally, in observations, uncertainties in the star-formation histories, dust content and distribution, the IMF, and other effects can easily introduce systematic errors of a factor of $\sim$2 in the SFRs, particularly at high redshift (see, e.g., Reddy et al. 2008; Muzzin et al. 2009; Wuyts et al. 2009). Even though nowadays there is reasonable agreement between the global stellar mass density inferred at any particular time and the time integral of all the preceding instantaneous star-formation activity, modest offsets may still point toward systematic uncertainties that are not negligible (see Madau & Dickinson 2014, for a review).

Moreover, the tensions seen between $1 < z < 1.5$ and $0.5 < z < 1$ in observations are at least partly due to the fact that our analysis relies on COSMOS data, which covers only one field of view. Therefore, we are not able to control for sample variance. Guzzo et al. (2007) identified a large-scale structure at $z \sim 0.73$, which certainly contaminates the counts at $0.5 < z < 1$, most probably having an impact on the mass functions and on the cumulative number densities involved in the selection of the progenitors. Having a larger sample of galaxies, based on several fields, is mandatory to really prove the existence of the observed gap and to understand its origin.

8. SUMMARY AND CONCLUSIONS

The aim of this paper was to test the model predictions for the different contributions to the stellar mass assembly since $z \sim 2$, and investigate the role of the star formation and mergers at the different redshifts. We compared observational results with the data of two different semi-analytic models, to obtain a better insight on the physical processes responsible for the evolution.

First, we characterized the environment of the progenitors of local UMGs at $0.2 < z < 2$, selected with a semi-empirical approach using abundance matching in the ΛCDM paradigm (Behroozi et al. 2013; Marchesini et al. 2014). We investigated the number of companions around each progenitor, in order to give an estimate of the environment surrounding these massive galaxies. The number of galaxies with mass at least 1:10 the mass of the progenitor and with redshift within $\pm 0.05 \times (1 + z_{\rm pr})$ around progenitors depends on distance. In observations, at any redshift $\sim$80% of the progenitors have no galaxies within a projected radius of 50 kpc. This number drops to 25% at $z \sim 1.75$% and 5% at lower redshift when a radius of 500 kpc is considered. In general, going from higher to lower redshift, the environment gets proportionally richer of companions. Models qualitatively agree with observations, even though the fraction of isolated progenitors is much lower in the models, indicating progenitors live in denser environments and pointing to the well known over-estimation of satellites at high redshift (in the DLB07 model).

Considering only progenitors with at least one companion within 500 kpc, in both observations and simulations the number of companions decreases with distance. Nonetheless, the DLB07 model overestimates the number of companions at almost all distances (in agreement with previous results, e.g., Weinmann et al. 2011; Vulcani et al. 2014). The star-forming properties of progenitors and companions do not seem to influence the trends in observations, while in models the fraction of quiescent companions might be higher around quiescent progenitors.

In the second part of the paper we investigated which factors are the most important in the progenitors' mass growth at the

different redshifts, characterizing the separate contribution of star formation and mergers.

Overall, our analysis confirms the model predictions, showing how the growth history of massive galaxies is dominated by in situ star formation at $z \sim 2$, both star formation and mergers at $1 < z < 2$, and by mergers alone at $z < 1$. Nonetheless, detailed comparisons reveal some tension between the mass growth expected by the abundance matching technique and that measured both in observations and in simulations. In observations, we recover a systematically smaller mass growth when SFRs from SED fitting are adopted, whereas we obtain an overall comparable mass growth when SFRs from UV+IR are used. The true mass growth has to be bracketed between these two cases. In models, both prescriptions explain the mass growth as predicted by the abundance matching technique, and, when errors are taken into account even overpredict it. The role of the different contributions is different in the two prescriptions, highlighting how much the mass growth is model dependent. It is worth noticing that the mass growth estimated for the H15 model and the one that is intrinsic in the model are not in agreement. This implies that at least some of the assumptions made to estimate the different contribution to mass growth could be wrong.

Discrepancies might be due to a number of factors, such as an incorrect progenitors-descendants selection, an underestimate of minor mergers (>1:10), the adopted assumptions on merger rates, or uncertainties on SFR and mass estimates.

In the future, a larger sample of observed galaxies will be needed to draw more robust conclusions. Indeed, the non-negligible spread measured among the different extractions in simulations indicates that the sample variance is not marginal. A larger sample would also allow us to better investigate the impact of the environmental processes on galaxy evolution. It has been shown that the efficiency and the timescale of the quenching of star formation in satellites is halo mass dependent, therefore at any redshift the role of star formation is certainly different in different environments (e.g., Dekel & Birnboim 2006; Dekel et al. 2009).

Another natural step forward to this analysis will be to better characterize the gas content and the interstellar medium (ISM) in the progenitors' population, especially in the star-forming progenitors, during a period in cosmic history that is most critical for the formation of their stars ($1 < z < 3$). Observation (e.g., with ALMA) will allow us to carefully investigate the ISM, which is the crucial ingredient fueling the activities of star formation and AGNs, and separating the two contributions will better constrain the actual role of star formation in the total mass growth.

We thank the referee for comments that helped us improve the manuscript. B.V. acknowledges support from the World Premier International Research Center Initiative (WPI), MEXT, Japan, and the Kakenhi Grant-in-Aid for Young Scientists (B) (26870140) from the Japan Society for the Promotion of Science (JSPS). D.M. acknowledges the support of the Research Corporation for Science Advancement's Cottrell Scholarship. B.M.J. acknowledges support from the ERC-StG grant EGGS-278202. The Dark Cosmology Centre is funded by the DNRF. This study is based on data products from observations made with ESO Telescopes at the La Silla Paranal Observatory under ESO programme ID 179.A-2005 and on data products produced by TERAPIX and the Cambridge Astronomy Survey Unit on behalf of the UltraVISTA consortium. The Millennium Simulation databases used in this paper and the web application providing online access to them were constructed as part of the activities of the German Astrophysical Virtual Observatory (GAVO). I.L. and M.S. acknowledge the support from NL-NWO Spinoza.

REFERENCES

Behroozi, P. S., Marchesini, D., Wechsler, R. H., et al. 2013, ApJL, 777, L10
Bell, E. F., Naab, T., McIntosh, D. H., et al. 2006, ApJ, 640, 241
Berrier, J. C., Bullock, J. S., Barton, E. J., et al. 2006, ApJ, 652, 56
Bildfell, C., Hoekstra, H., Babul, A., et al. 2012, MNRAS, 425, 204
Blanton, M. R., & Moustakas, J. 2009, ARA&A, 47, 159
Brammer, G. B., Whitaker, K. E., van Dokkum, P. G., et al. 2011, ApJ, 739, 24
Brough, S., Tran, K.-V., Sharp, R. G., von der Linden, A., & Couch, W. J. 2011, MNRAS, 414, L80
Bruzual, G., & Charlot, S. 2003, MNRAS, 344, 1000
Burke, C., Hilton, M., & Collins, C. 2015, MNRAS, 449, 2353
Calzetti, D., Armus, L., Bohlin, R. C., et al. 2000, ApJ, 533, 682
Capak, P., Aussel, H., Ajiki, M., et al. 2007, ApJS, 172, 99
Cimatti, A., Cassata, P., Pozzetti, L., et al. 2008, A&A, 482, 21
Collins, C. A., Stott, J. P., Hilton, M., et al. 2009, Natur, 458, 603
Conroy, C., & Wechsler, R. H. 2009, ApJ, 696, 620
Conroy, C., Wechsler, R. H., & Kravtsov, A. V. 2006, ApJ, 647, 201
Conroy, C., Wechsler, R. H., & Kravtsov, A. V. 2007, ApJ, 668, 826
Croton, S. D. M., Springel, D. J., White, V., et al. 2006, MNRAS, 365, 11
Dekel, A., & Birnboim, Y. 2006, MNRAS, 368, 2
Dekel, A., Birnboim, Y., Engel, G., et al. 2009, Natur, 457, 451
De Lucia, G., & Blaizot, J. 2007, MNRAS, 375, 2
De Lucia, G., Kauffmann, G., Springel, V., et al. 2004a, MNRAS, 348, 333
De Lucia, G., Poggianti, B. M., Aragón-Salamanca, A., et al. 2004b, ApJL, 610, L77
De Lucia, G., Springel, V., White, S. D. M., Croton, D., & Kauffmann, G. 2006, MNRAS, 366, 499
Drory, N., & Alvarez, M. 2008, ApJ, 680, 41
Dullo, B. T., & Graham, A. W. 2013, ApJ, 768, 36
Ferreras, I., Trujillo, I., Mármol-Queraltó, E., et al. 2014, MNRAS, 444, 906
Fontanot, F., De Lucia, G., Monaco, P., Somerville, R. S., & Santini, P. 2009, MNRAS, 397, 1776
Gao, L., White, S. D. M., Jenkins, A., Stoehr, F., & Springel, V. 2004, MNRAS, 355, 819
George, M. R., Leauthaud, A., Bundy, K., et al. 2011, ApJ, 742, 125
Gobat, R., Daddi, E., Béthermin, M., et al. 2015, arXiv:1507.03953
Graham, A. W. 2013, in Planets, Stars, and Stellar Systems. Volume 6: Extragalactic Astronomy and Cosmology, ed. T. D. Oswalt & W. C. Keel (Berlin: Springer), 91
Graham, A. W., Dullo, B. T., & Savorgnan, G. A. D. 2015, ApJ, 804, 32
Guo, Q., White, S., Boylan-Kolchin, M., et al. 2011, MNRAS, 413, 101
Guo, Q., & White, S. D. M. 2008, MNRAS, 384, 2
Guzzo, L., Cassata, P., Finoguenov, A., et al. 2007, ApJS, 172, 254
Henriques, B. M. B., White, S. D. M., Thomas, P. A., et al. 2015, MNRAS, 451, 2663
Ilbert, O., McCracken, H. J., Le Fèvre, O., et al. 2013, A&A, 556, A55
Kitzbichler, M. G., & White, S. D. M. 2008, MNRAS, 391, 1489
Kravtsov, A. V., Berlind, A. A., Wechsler, R. H., et al. 2004, ApJ, 609, 35
Kroupa, P. 2001, MNRAS, 322, 231
Labbé, I., Bouwens, R., Illingworth, G. D., & Franx, M. 2006, ApJL, 649, L67
Leja, J., van Dokkum, P., & Franx, M. 2013, ApJ, 766, 33
Lidman, C., Iacobuta, G., Bauer, A. E., et al. 2013, MNRAS, 433, 825
Lidman, C., Suherli, J., Muzzin, A., et al. 2012, MNRAS, 427, 550
Lin, Y.-T., Brodwin, M., Gonzalez, A. H., et al. 2013, ApJ, 771, 61
López-Sanjuan, C., Le Fèvre, O., Ilbert, O., et al. 2012, A&A, 548, A7
Ma, C.-P., Greene, J. E., McConnell, N., et al. 2014, ApJ, 795, 158
Madau, P., & Dickinson, M. 2014, ARA&A, 52, 415
Marchesini, D., Muzzin, A., Stefanon, M., et al. 2014, ApJ, 794, 65
Marín, F. A., Wechsler, R. H., Frieman, J. A., & Nichol, R. C. 2008, ApJ, 672, 849
Martin, D. C., Fanson, J., Schiminovich, D., et al. 2005, ApJL, 619, L1
McCracken, H. J., Milvang-Jensen, B., Dunlop, J., et al. 2012, A&A, 544, A156
McIntosh, D. H., Guo, Y., Hertzberg, J., et al. 2008, MNRAS, 388, 1537
Mundy, C. J., Conselice, C. J., & Ownsworth, J. R. 2015, MNRAS, 450, 3696
Muñoz-Cuartas, J. C., Macciò, A. V., Gottlöber, S., & Dutton, A. A. 2011, MNRAS, 411, 584

Muzzin, A., Marchesini, D., Stefanon, M., et al. 2013a, ApJS, 206, 8
Muzzin, A., Marchesini, D., Stefanon, M., et al. 2013b, ApJ, 777, 18
Muzzin, A., Marchesini, D., van Dokkum, P. G., et al. 2009, ApJ, 701, 1839
Naab, T., Johansson, P. H., & Ostriker, J. P. 2009, ApJL, 699, L178
Naab, T., Johansson, P. H., Ostriker, J. P., & Efstathiou, G. 2007, ApJ, 658, 710
Ownsworth, J. R., Conselice, C. J., Mortlock, A., et al. 2014, MNRAS, 445, 2198
Papovich, C., Moustakas, L. A., Dickinson, M., et al. 2006, ApJ, 640, 92
Patel, S. G., Kelson, D. D., Holden, B. P., Franx, M., & Illingworth, G. D. 2011, ApJ, 735, 53
Poggianti, B. M., Moretti, A., Calvi, R., et al. 2013, ApJ, 777, 125
Puchwein, E., Springel, V., Sijacki, D., & Dolag, K. 2010, MNRAS, 406, 936
Quilis, V., & Trujillo, I. 2012, ApJL, 752, L19
Rasmussen, J., Mulchaey, J. S., Bai, L., et al. 2010, ApJ, 717, 958
Reddy, N. A., Steidel, C. C., Pettini, M., et al. 2008, ApJS, 175, 48
Rider, P. R. 1960, JASA, 55, 148
Ruiz, P., Trujillo, I., & Mármol-Queraltó, E. 2014, MNRAS, 442, 347
Sánchez, A. G., Baugh, C. M., Percival, W. J., et al. 2006, MNRAS, 366, 189
Sanders, D. B., Salvato, M., Aussel, H., et al. 2007, ApJS, 172, 86
Shankar, F., Buchan, S., Rettura, A., et al. 2015, ApJ, 802, 73
Springel, V., White, S. D. M., Jenkins, A., et al. 2005, Natur, 435, 629
Springel, V., White, S. D. M., Tormen, G., & Kauffmann, G. 2001, MNRAS, 328, 726
Tal, T., Quadri, R. F., Muzzin, A., Marchesini, D., & Stefanon, M. 2014, arXiv:1405.4856
Tal, T., van Dokkum, P. G., Franx, M., et al. 2013, ApJ, 769, 31
Tal, T., Wake, D. A., van Dokkum, P. G., et al. 2012, ApJ, 746, 138
Tasitsiomi, A., Kravtsov, A. V., Wechsler, R. H., & Primack, J. R. 2004, ApJ, 614, 533
Thomas, D., Maraston, C., Bender, R., & Mendes de Oliveira, C. 2005, ApJ, 621, 673
Tinker, J. L., George, M. R., Leauthaud, A., et al. 2012, ApJL, 755, L5
Torrey, P., Wellons, S., Machado, F., et al. 2015, MNRAS, 454, 2770
Tran, K.-V. H., van Dokkum, P., Franx, M., et al. 2005, ApJL, 627, L25
Trujillo-Gomez, S., Klypin, A., Primack, J., & Romanowsky, A. J. 2011, ApJ, 742, 16
Vale, A., & Ostriker, J. P. 2004, MNRAS, 353, 189
Vale, A., & Ostriker, J. P. 2006, MNRAS, 371, 1173
van Dokkum, P. G. 2005, AJ, 130, 2647
van Dokkum, P. G. 2008, ApJ, 674, 29
van Dokkum, P. G., Franx, M., Fabricant, D., Kelson, D. D., & Illingworth, G. D. 1999, ApJL, 520, L95
van Dokkum, P. G., Franx, M., Förster Schreiber, N. M., et al. 2004, ApJ, 611, 703
van Dokkum, P. G., & van der Marel, R. P. 2007, ApJ, 655, 30
van Dokkum, P. G., Whitaker, K. E., Brammer, G., et al. 2010, ApJ, 709, 1018
Vulcani, B., De Lucia, G., Poggianti, B. M., et al. 2014, ApJ, 788, 57
Wake, D. A., Nichol, R. C., Eisenstein, D. J., et al. 2006, MNRAS, 372, 537
Wang, L., Li, C., Kauffmann, G., & De Lucia, G. 2006, MNRAS, 371, 537
Wang, Y., Yang, X., Mo, H. J., & van den Bosch, F. C. 2007, ApJ, 664, 608
Weinmann, S. M., Lisker, T., Guo, Q., Meyer, H. T., & Janz, J. 2011, MNRAS, 416, 1197
Wetzel, A. R., Cohn, J. D., & White, M. 2009, MNRAS, 395, 1376
Whitaker, K. E., Labbé, I., van Dokkum, P. G., et al. 2011, ApJ, 735, 86
White, M., Zheng, Z., Brown, M. J. I., Dey, A., & Jannuzi, B. T. 2007, ApJL, 655, L69
Williams, R. J., Quadri, R. F., Franx, M., van Dokkum, P., & Labbé, I. 2009, ApJ, 691, 1879
Wuyts, S., Franx, M., Cox, T. J., et al. 2009, ApJ, 696, 348
Wuyts, S., Labbé, I., Franx, M., et al. 2007, ApJ, 655, 51
Yamada, T., Koyama, Y., Nakata, F., et al. 2002, ApJL, 577, L89
Zehavi, I., Patiri, S., & Zheng, Z. 2012, ApJ, 746, 145